UNIVERSITA' POLITECNICA DELLE MARCHE

FACULTY OF ENGINEERING

Master's degree course in Biomedical Engineering

STUDY OF THE WETTABILITY OF FERROELECTRIC FLUID ON FERROELECTRIC CRYSTALS

Supervisor:

Prof. Lucchetti Liana

Candidate:

Zigrossi Gianfranco

Academic Year 2021 / 2022

Abstract

The objective of the thesis is the study of the wettability of the newly discovered liquid crystalline material 4-[(4-nitrophenoxy)carbonyl]phenyl 2,4-dimethoxybenzoate (RM734), on different kinds of ferroelectric solid surfaces. RM734 is the first liquid crystal that exhibits a ferroelectric nematic phase, which makes it the first ferroelectric liquid material ever observed. The fluid nature of this new phase combined with its polarity, makes its response to electric fields stronger and intrinsically different with respect to both ferroelectric solids and dielectric fluids. When in contact with solid substrates, the RM734 polarization P is always parallel to the surface, no matter its chemistry, since any other direction would lead to an energetically costly accumulation of surface charge $\sigma = P \cdot u$, u being a unit vector normal to the surface. It is thus of particular interest to investigate the behavior at the interface between RM734 and ferroelectric solids, a situation that we have here studied by depositing sessile liquid crystal droplets on different ferroelectric substrates. Specifically, we have studied the wettability of RM734 drops on different Lithium Niobate substrates with different iron doping levels and different reduction factors, extracting the contact angle as a function of temperature. Results demonstrated that this particular liquid crystal behaves differently on different types of substrates, giving rise to peculiar behaviors, from abrupt changes of the contact angle upon entering the ferroelectric nematic phase, to sudden emission of interfacial fluid jets.
Our study contribute an additional piece to the collection of intriguing features characterizing the ferroelectric nematic phase and may have potential for future applications.

Index

Index of figures

DREAM ON

INTRODUCTION

Liquid crystal (LC) is nowadays a very commonly used term but, like many other words imported from scientific literature into common life, it is poorly understood in its deep meaning. The difference between crystals and liquids, the two most common condensed matter phases, is that the molecules in a crystal are ordered whereas in a liquid they are not. The order in a crystal is both positional and orientational, in that the molecules are constrained both to occupy specific sites in a lattice and to point their molecular axes in specific directions. The molecules in liquids, on the other hand, diffuse randomly throughout the sample container with the molecular axes tumbling wildly. Interestingly enough, there are also in nature many phases with more order than those present in liquids but less order than that typical of crystals. The molecules in all liquid crystal phases diffuse about much like the molecules of a liquid, but as they do so they maintain some degree of orientational order and sometimes some positional order also. The amount of order in a liquid crystal is quite small relative to a crystal. There is only a slight tendency for the molecules to point more in one direction than others or to spend more time in various positions than others. Depending on the amount and on the kind of order, several different liquid crystal phases can be identified. The simplest and more similar to a conventional liquid is the nematic phase, which is at the basis of the liquid crystal display technology. In the conventional nematic phase, rod-shaped molecules are orientationally aligned with respect to each other. Nevertheless, the phase in not polar as the probabilities that molecular dipoles are pointing in each of the two opposite directions associated with the alignment axis are the same [1]. Recently, nematic liquid crystal compounds exhibiting polar order were discovered [2]. This is an important discovery since the combination of fluidity and polar coupling to electric fields, peculiar of this new phase, is opening the gate to a whole new world of phenomena, which are rapidly becoming the focus of the liquid crystals and soft material scientific communities. The ferroelectric nematic liquid phase was first recognized in the phase diagram of RM734, a compound observed to feature an unexpected second nematic phase, later proved to exhibit self-stabilized spontaneous polar order. The discovery of the molecule DIO and of structural variants of RM734 has recently led to the identification of additional families of ferroelectric-forming materials, some of which operating at room temperature. Beside adding a new, very peculiar, member to the group of ferroelectric materials, the new phase offers a broad range of physical effects to explore, ranging from the behavior of topological defects to surface anchoring, response to low frequency electric fields and light, interplay of bound and free electric charges, viscoelastic properties, field-controlled hydrodynamics, field-order coupling in both the ferroelectric and the pre-transitional regions, behavior in confined geometry, just to cite a few examples.

In this scenario, the research proposed here focus on the behavior of sessile ferroelectric liquid droplets deposited on ferroelectric solid substrates. The wettability of RM734 was studied as a function of temperature, by analyzing the behavior of the droplets contact angle. This study has been inspired by recent observations performed by our research group, showing that the coupling between the polarizations of the fluid and solid materials, gives rise to peculiar effects. Specifically, upon entering the ferroelectric phase by reducing the temperature from the nematic phase, the liquid crystal droplets undergo an electromechanical shape instability and disintegrate by the explosive emission of fluid jets [3]. The role played in the phenomenon by the combination of surface tension and

polarization charge accumulation, although certainly relevant, was not totally clear. A detailed analysis of the liquid crystal wettability on different ferroelectric substrates, was thus scheduled to clarify the point.

The thesis is structured as follows: Chapter 1 describes liquid crystalline materials and the ferroelectric crystal used in our experiments. It also reports the concept of contact angle and the description of the ferroelectric droplet instability. Chapter 2 contains the description of the performed measurements. Chapter 3 describes the procedure of image analysis leading to the computation of the droplet contact angle. Chapter 4 reports the experimental results, which are then discussed in Chapter 5.

CHAPTER 1

1. LIQUID CRYSTALS

1.1 GENERAL DESCRIPTION

All of us have learned that matter can only exist in three different states: solid, liquid, and gas. This is not entirely accurate. Particularly, some organic materials exhibit a cascade of transitions incorporating new phases rather than a single transition from solid to liquid. Mechanical and symmetry characteristics of these phases lie between those of a liquid and those of a crystal. For this reason, they are frequently referred as liquid crystals. Liquid crystals are a state of matter, which can be made by systems composed of different types of molecules in which the most common ones are elongated molecules with aromatic rings. The presence of organic rings, made up of carbon atoms and many delocalized electrons, governs all the main physical properties that characterize liquid crystals such as: dielectric and elastic constants, viscosity, non-linear optical effects and anisotropy. As an example, Fig. 1 reports the structure of 4-Cyano-4'-pentylbiphenyl (5CB), one of the most studied LC compounds that exhibiting a nematic LC phase at room temperature.

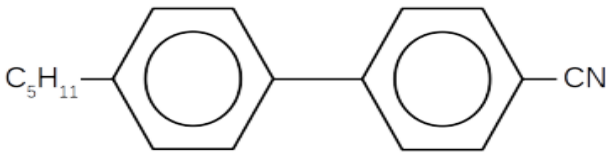

Figure 1. Molecular structure of 5CB liquid crystals

The crystals can be observed in three main phases, depending on the temperature in which are found as we will see in more detail in the next sections. At room temperature (in a range that covers about 10-20°C) most of the liquid crystals are in the nematic phase, in which their shape enjoys axial symmetry (they are uniaxial crystals). At lower temperatures the crystals are in the solid or smectic phase, the latter characterized by the organization of crystals in layers parallel to each other. At higher temperatures, however, they are in the isotropic phase, in which they are randomly oriented. The order parameter that defines the transition from nematic phase to isotropic phase is given from:

$$S = \frac{1}{2} < 3\cos^2(\theta_i - 1)$$

Where θ_i is the angle formed by a given molecule and an arbitrarily chosen direction and the average is performed on all the liquid crystals contained in the considered system. S is non-zero for the nematic phase, while it is equal to zero for the isotropic phase.

1.2 TYPES OF LIQUID CRYSTALS

There are two types of liquid crystal mesophases that must be differentiated, thermotropic which are pure compounds and lyotropic which are macromolecules in solution, typically in water. Thermotropic liquid crystals are of interest both from standpoint of basic research and also for applications in electro-optic displays, temperature and pressure sensors. The lyotropic liquid crystals, on the other hand, are of great interest in biology and appear to play an important role in living systems.

As for thermotropic liquid crystals, the term "thermotropic" arises because transitions involving these mesophases are most naturally affected by changing temperature. Materials showing thermotropic liquid crystal phases are usually organic substances with molecular structures typified by those of cholesteryl nonanoate and N-(p-methoxybenzylidene) -p'-n-butylaniline (MBBA) shown in Figure 2.

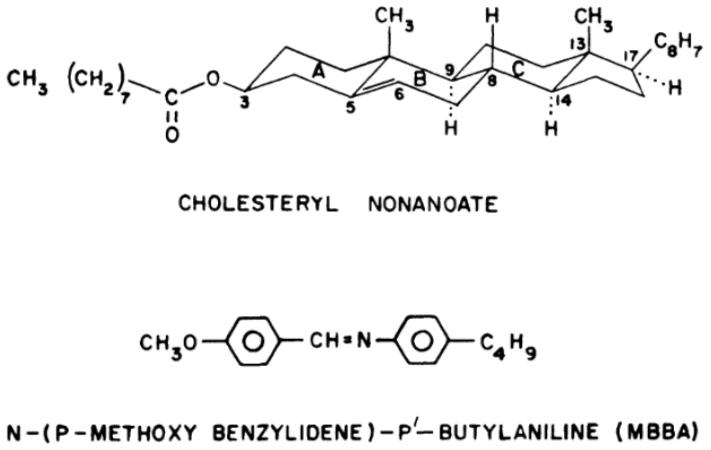

Figure 2. Example of molecular structures that give rise to thermotropic mesophases.

Axial ratios of 4-8 and molecular weights of 200-500 g/mol are typical for thermotropic liquid crystals mesogens. In this type of liquid crystal, every molecule participates on an equal basis in the long-range ordering.

Solutions of rod-like entities in a normally isotropic solvent often form liquid-crystal phases for sufficiently high solute concentration. These anisotropic solution mesophases are called "lyotropic liquid crystals". Although the rod-like entities are usually quite large compared to typical thermotropic liquid-crystal mesogens, their axial ratios are seldom greater than ~15. Deoxyribonucleic acid (DNA), certain viruses and many synthetic polypeptides all form lyotropic mesophases when dissolved in an appropriate solvent in suitable concentration. The conformation of most of these materials is quite temperature sensitive, i.e. the rods themselves are rather unstable with respect to temperature changes. This essentially eliminates the possibility of thermally inducing phase transitions involving lyotropic mesophases. A more natural parameter which can be varied to produce such transitions is the solute concentration. The principal interaction producing long range order in

lyotropic liquid crystals is the solute-solvent interaction; solute-solute interactions are of secondary importance. To a good approximation, then, only rod-like entities (solutes) participate in the long-range ordering [4].

1.3 LIQUID CRYSTAL PHASES

The liquid crystal state is a distinct phase of matter observed between the crystalline (solid) and isotropic (liquid) states. There are many types of liquid crystal states, depending upon the amount of order in the material. The nematic phase of calamitic liquid crystals is the simplest liquid crystal phase. In this phase the molecules maintain a preferred orientational direction as they diffuse throughout the sample. There is no positional order in this phase, and this is the phase represented in Figure 3 showing a representation of molecular order on the left and a polarized light microscopy image on the right. The term "nematic" comes from the Greek word for thread, since in a polarizing microscope there are often many dark lines visible in thick film samples. These lines are defects in the orientation order or points where the optical axis of the liquid crystal is parallel to the polarizers of the microscope and are called disclinations. The preferred direction is undefined at these disclinations.

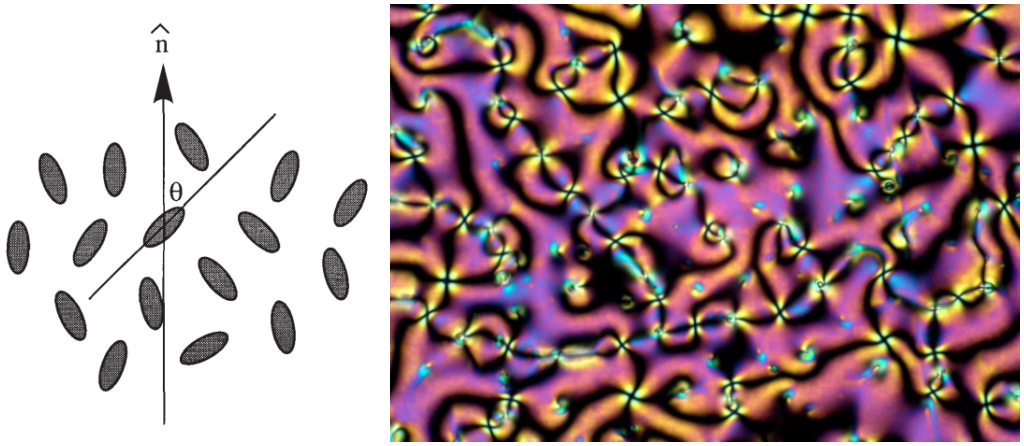

Figure 3. Molecular order in a nematic liquid crystal

Two other phases common to calamitic liquid crystals are shown in Figure 4. In addition to the orientational order of nematic, these phases exhibit positional order since the centers of mass of the rod-shaped molecules are arranged in layers. If the director is perpendicular to the layers in which molecules are more likely to be, the phase is called a smectic A liquid crystal. If the director makes an angle other than 90° to these layers, it is a smectic C phase. In these two phases, there is no positional order within the layers.

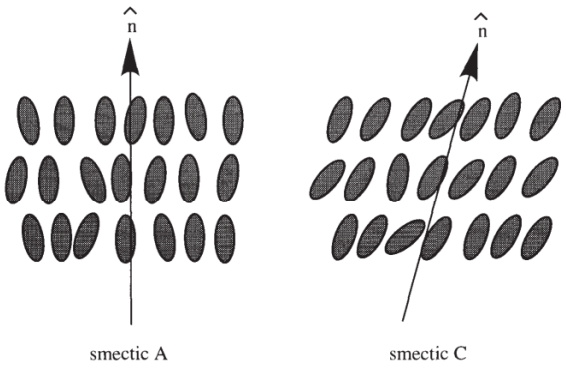

Figure 4. Two liquid crystal phases with positional order

The name smectic comes from the Greek word for soap since the mechanical properties of these phases reminded early researchers of soap systems. Over the years, many phases with the layering order of the smectic A and C phases have been discovered and called smectic liquid crystals. Some involve hexagonal or rectangular positional order in the plane of the layers but with no registry of this two-dimensional order from one layer to the next except for the directions of the axes of the rectangular or hexagonal lattice. This type of order has come to be known as bond orientational order, and the phases that possess it are called smectic hexatic phases. While all of these phases are proper liquid crystal phases, there are other phases in which the positional order is three dimensional. In these phases, the two-dimensional positional order carries from one layer to the next with respect to both the orientation and position of the lattice. Although such phases were originally labelled as smectic liquid crystals, they are now more properly called crystal mesophases. These layered phases also differ in the nature of the rotation of the molecules about their long axes. In many phases there is unhindered thermal rotation about the long axes of the molecules; in other phases the rotation is hindered with only 'flips' of 180° taking place.

If the molecules that form a liquid crystal phase are chiral (lack inversion symmetry), then chiral phases exist in place of certain non-chiral phases. In calamitic liquid crystals, the nematic phase is replaced by the chiral nematic phase, in which the director rotates in helical fashion about an axis perpendicular to the director. Such a phase is illustrated in Figure 5.

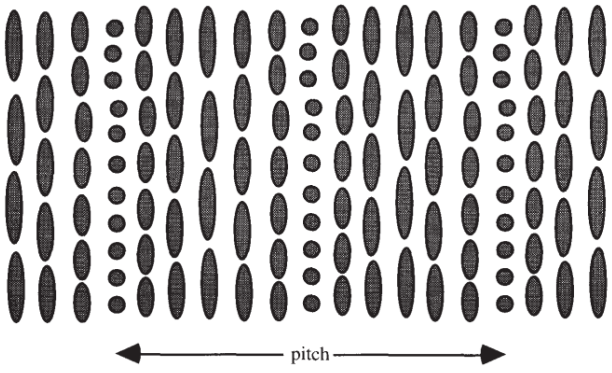

Figure 5. Structure of the chiral nematic phase

The pitch of a chiral nematic phase is the distance along the helix over which the director rotates by 360°. It should be noted, however, that the structure repeats itself every half pitch due to the equivalency of ***n*** and ***-n***. Finally, the chiral nematic phase is often called the cholesteric phase, since many of the first compounds that possessed this phase were derivatives of cholesterol [3].

1.4 BIREFRINGENCE

When light enters a material, its wavelength and velocity decrease by a factor called the index of refraction. An isotropic material has a single index of refraction since light polarized in any direction travels at the same velocity in the material. For example, the index of refraction of water is about 1.3 and of glass about 1.5. If n is the index of refraction of a material, then the wavelength and velocity of the light in the material are given by the following relations:

$$v = \frac{c}{n} \quad and \quad \lambda = \frac{\lambda_0}{n}$$

where λ_0 is the wavelength of the light in vacuum.

Liquid crystals are anisotropic materials and the refractive index seen by light travelling in a liquid crystalline material depends on the mutual direction between molecular director **n** and light polarization. Specifically, light polarized orthogonal to **n** sees the so called ordinary refractive index, lower with respect to the one experienced by light polarized along **n,** the extraordinary refractive index. Liquid crystal thus possesses two refractive indexes. This optical phenomenon is called birefringence, and since we are discussing linearly polarized light, it should really be called linear birefringence. Figure 6 shows how these two indices of refraction for a specific wavelength vary with temperature.

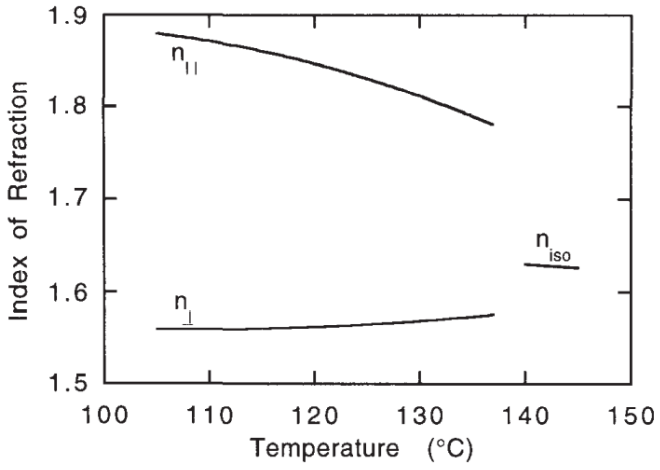

Figure 6. Indices of refraction for a typical for a typical nematic liquid crystal

The difference between the two indices of refraction $\Delta n = n_{//} - n_{\perp}$, (called optical anisotropy or birefringence) is related to the amount of order of the liquid crystal phase. Clearly shows the fact that the order parameter decreases with increasing temperature. In fact, Δn follows the variation of the order parameter as Figure 7 demonstrates.

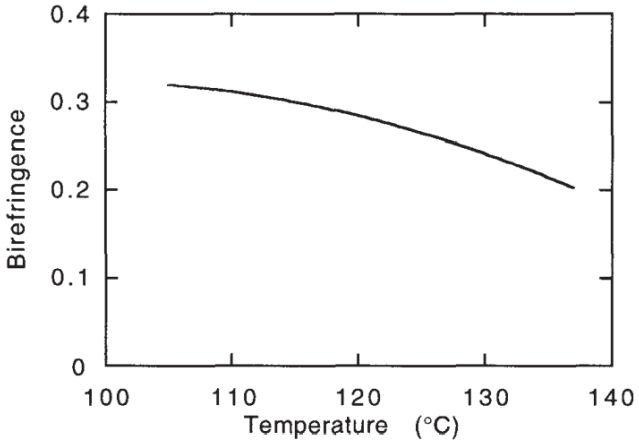

Figure 7. Birefringence for a typical nematic liquid crystal

Birefringence is a property of all anisotropic materials, whether uniaxial or biaxial. Nematic liquid crystals fall into the uniaxial category along with crystals of hexagonal, tetragonal, and trigonal symmetry. If the optical anisotropy is positive (n_e is greater than n_0 in a uniaxial system), the material is said to be positive uniaxial. If the opposite is true, the material is negative uniaxial.

1.5 OPTICAL POLARISING MICROSCOPY

The optical polarizing microscopy enables the identification of the liquid crystal phases on the basis of the observed optical texture. The technique is also essential when evaluating the physical properties of liquid crystals in certain phases and in specific temperature ranges. The identification of mesophases through optical polarizing microscopy usually involves the magnified view of a thin sample of a mesogenic material sandwiched between two glass microscope slides. The obtained LC cell is usually placed on the microscope stage, which can be accurately temperature-controlled, and observed between crossed polarizers. If an isotropic liquid is analyzed, the polarized light remains unaffected by the sample (since it is isotropic) and so no light passes through the second polarizer (called the analyzer). However, when an anisotropic, birefringent medium is present, light is not extinguished, and an optical texture appears that gives information relating to the average arrangement of the molecules within the medium. When analyzing mesophases by optical polarizing microscopy, the texture that is revealed depends upon how the sample is aligned, in addition to being dependent upon the phase structure of the sample. There are two basic forms of alignment for liquid crystalline compounds, homeotropic and homogeneous (planar), that are represented in Figure 8.

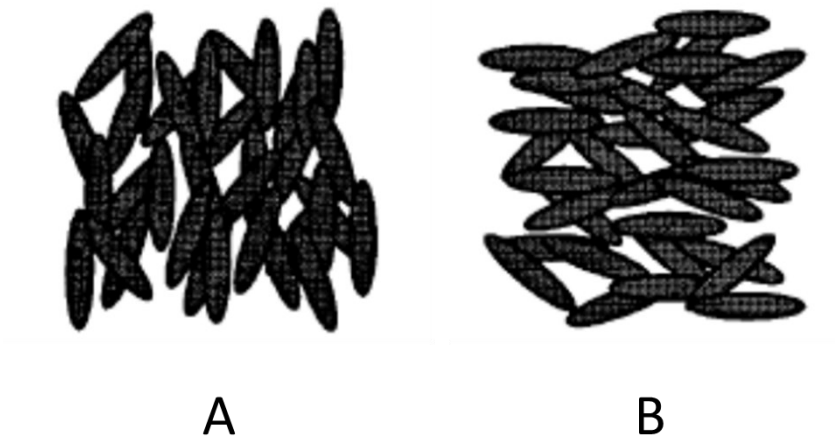

Figure 8. Homeotropic (A) and Homogeneous (B) alignment of liquid crystals

Homeotropic alignment is obtained when the liquid crystal molecules are oriented such that their long axes (whose average orientation defines the optic axes) are normal to the supporting substrate. When the molecules are oriented in this way, light polarized in the plane orthogonal to the optic axis, is unaffected by the material and cannot pass through the analyzer. In these conditions, sample will appear dark. In homogeneous (planar) alignment the constituent molecules of the liquid crystal phase are on the average oriented parallel to the supporting substrates. With homogeneous alignment, a thin film of the liquid crystal phase exhibits birefringence and a colored texture results when viewed between crossed polarisers. However, where the long molecular axes are in line with either polariser, light is extinguished.

1.6 FERROELECTRIC LIQUID CRYSTALS

Until recently, the only polar liquid crystalline materials were the Smectic-C*, which possess nonzero spontaneous polarization $\vec{\boldsymbol{P}}$. In these kind of liquid crystals ferroelectricity is determined by molecular chirality [5] and some smectic phase formed by achiral bent-core molecules [6] have also been observed, both with a viscosity too high to be really considered "liquid".

Very recently, the observation of a low viscous nematic polar phase has been reported, in which the spontaneous polarization arises due to the orientation of all the molecular dipoles in the same direction in a nematic configuration [5]. This phase is called the ferroelectric nematic phase (N_F) and was firstly observed in the compound of 4-[(4-nitrophenoxy)carbonyl]phenyl 2,4-dimethoxybenzoate (RM734). This is a very important discovery since the combination of fluidity and polar coupling to electric fields is opening the gate to a whole new world of phenomena, which are rapidly becoming the focus of the liquid crystal and soft material scientific communities. The ferroelectric nematic phase displays a slew of unique properties, all related to the combination between fluidity and polarity: they are extremely responsive to electric fields, exhibit very peculiar elastic properties, have large nonlinear optical susceptibility, can guide electric fields and more peculiar features are going to be unveiled. 4-

[(4-nitrophenoxy)carbonyl]phenyl 2,4-dimethoxybenzoate (RM734) is the ferroelectric nematic liquid crystal used in this thesis.

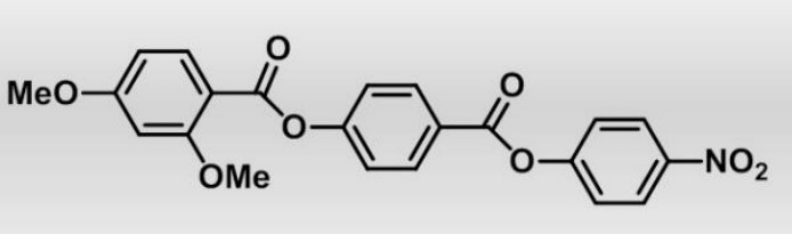

Figure 9. Structure of RM734

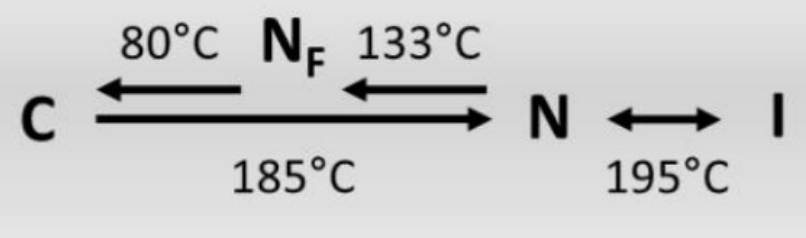

Figure 10. Phase diagram of RM734

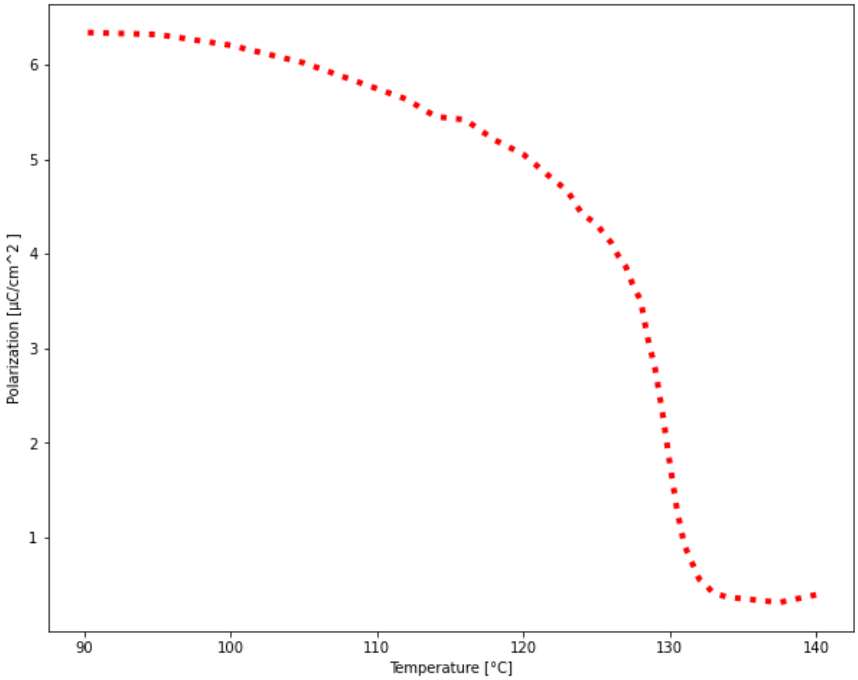

Figure 11. P vs T graph

The ferroelectric nematic (N_F) phase of RM734 appears through a second order phase transition upon cooling from the conventional N phase. The spontaneous polarization **P** of this compound depends on temperature and exceeds 6 $\mu C / cm^2$ at the lowest temperature in the N_F phase. Being both related to molecular order, the polarization and the nematic director are in the same direction and **P** is either parallel or antiparallel to the molecular director **n.**

A very peculiar property of the ferroelectric nematic phase, which is a consequence of the combination of large spontaneous polarization and fluidity, is the readiness with which it can accumulate surface charges of density $\mathbf{P} \cdot \mathbf{u}$ at any interface, either with solid walls or with air, by small collective rotations of **n** (**u** is a unit vector perpendicular to the surface). It is thus of particular interest to investigate the behavior at the interface between a NF phase and a ferroelectric solid, a situation that can be studied by depositing sessile LC droplets on a ferroelectric substrate.

In chapter three, we'll explore how temperature variations affect the liquid crystal RM734's contact angle with a ferroelectric solid and how this is related to the phenomenon of shape instability.

2. LITHIUM NIOBATE

In our study, lithium niobate (LN) is the ferroelectric crystal chosen as a substrate to deposit the ferroelectric RM734 droplets. Besides having a permanent polarization in the temperature range of interest, dictated by the RM734 phase diagram, LN is also an excellent substrate for the active control of matter, thanks to its remarkable pyroelectric effect and photovoltaic properties. Indeed, both temperature variations and visible light irradiation of LN have been proved to enable the realization of virtual, reconfigurable electrodes suitable for liquids, droplets and micro-objects manipulation [7]. In this thesis work undoped lithium niobate substrates and iron doped lithium niobate substrates with different reduction factor values were used.

1.2.1 CRYSTALLINE STRUCTURE

The crystalline structure of lithium niobate can be represented by equidistant planes on which the oxygen atoms are located forming equilateral triangles and rotated about 180° as shown in figure 12:

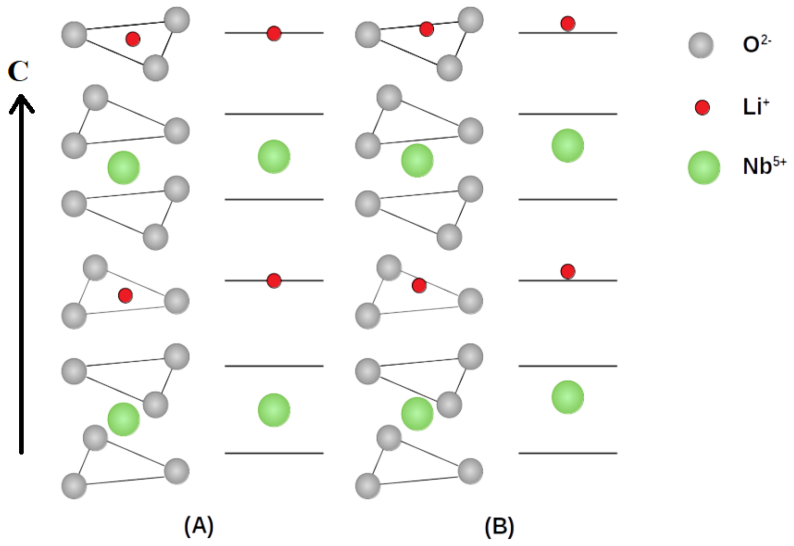

Figure 12. Crystal structure of lithium niobate in paraelectric (A) and ferroelectric (B) phase

In such a structure the position of the niobium and lithium ions depends on temperature. For temperatures above the Curie temperature (T_C = 1210°C), the crystal is in the paraelectric phase, with lithium ions in the center of the oxygen triangles and niobium ions in the center of the octahedron formed by two triangles on adjacent planes. For temperatures below T_C lithium and niobium move slightly along the optic axis of the crystal, also known as $\hat{\boldsymbol{c}}$ axis, resulting in a net polarization within the crystal. In this phase, which is polar and ferroelectric, LN exhibits symmetry of rotation of order three around the crystallographic axis $\hat{c}$ and symmetry by reflection with respect to three planes passing through $\hat{\boldsymbol{c}}$ and separated by 60° from each other.

1.2.2 PYROELECTRICITY

Pyroelectricity is a property exhibited by some crystals that have spontaneous electric polarization and gives rise to large internal electric fields. It can be described as the ability of certain materials to generate a temporary voltage when heated or cooled. The change in temperature slightly changes the position of the atoms within the crystalline structure, such that the polarization of the material changes. This change in polarization gives rise to a voltage across the crystal. If the temperature remains constant at its new value, the pyroelectric voltage gradually disappears due to leakage current (the leakage may be internal due to electrons moving through the crystal, or external due to ions moving in the air).

Below the Curie temperature, lithium niobate exhibits a spontaneous polarization, $\overrightarrow{\boldsymbol{P_s}} = \boldsymbol{P_s} \cdot \hat{\boldsymbol{k}}_{\boldsymbol{s}}$ along the polar axis $\hat{\boldsymbol{c}}$, which varies as a function of temperature.

The pyroelectric constant (λ) is defined as:

$$\lambda = \frac{dP_s}{dT}$$

and is equal to $\lambda = -4{,}0 \times 10^{-5}\ [\frac{C}{K \times m^2}]$ at room temperature [8]. The negative sign indicates that, in the cooling process, the face corresponding to the positive direction of the $\hat{\boldsymbol{c}}$ axis is charged positively. This charge distribution leads to the formation of a pyroelectric field which depends on the temperature change ΔT according to the relationship [8]:

$$\vec{E}_{pyro} = -\frac{1}{\varepsilon \varepsilon_0}\, \lambda\, \Delta T\, \vec{k}_s$$

and has an orientation antiparallel to the direction of the spontaneous polarization of the crystal ($\vec{\boldsymbol{k}}_{\boldsymbol{s}}$). Such a field can also be generated in the crystal under illumination due to local heating leading to a change in spontaneous polarization [7].

3. THE SHAPE INSTABILITY OF RM734 FERROELECTRIC DROPS

Interesting phenomena occur at the interface between a liquid crystal in the ferroelectric nematic (N_F) phase and a ferroelectric solid. In fact, the coupling of the two polarizations at the interface can give rise to effects on the wettability and on the contact angle of the droplet. Studies concerning these phenomena have been carried out and recently reported in PNAS [3]. In this paper, droplets contact angle was measured as a function of the substrate temperature on cooling from the isotropic (I) phase into the nematic (N) and N_F phases. As the temperature T is lowered, the contact angle mildly decreases in the I and N phases, signifying a slight increase of the wettability. Upon entering the N_F phase, the contact angle abruptly decreases followed by a sort of droplet explosion characterized by the ejection of jets of fluid, which branch out into smaller streams and eventually, disrupt into small new droplets. As T further decreases, these secondary droplets explode on their turn. This behavior is analog of the instability predicted by Lord Rayleigh for charged conductive liquid droplets above a critical charge-to-volume ratio. This instability arises from competing electrostatic and surface tension forces and leads to the formation of charge carrying fluid jets that reduce the droplet electric charge. The instability of ferroelectric sessile droplets on LN surfaces combines features typical of the Rayleigh instability, such as the ejection and retraction of jets and the formation of secondary droplets, with features due to it being driven by polarization, such as the repeated instability, the molecular order within the jets, and the T dependence of the explosions, which reflects the T dependence of P in the N_F phase. Additional instability features are related to the LC ordering, such as the coupling between birefringence and polarization, which offers a tool to characterize jets, and the relevant viscosity ranging between 0.05 and 3 Pa·s depending on T.

This dramatic manifestation of the interaction between the ferroelectric LC and the ferroelectric substrate is observed at a temperature that, for fixed cooling rate, mainly depends on the droplet's size and to a lower extent, the specific LN substrate. The appearance of these events upon entering the N_F phase suggests that they are an electrostatically driven phenomenon, but they are driven solely by the N_F / LN interaction, with no other sources of potential or electric field. An example of such a sudden explosion on an undoped substrate is shown in Figure 13 A and B (top and side views, respectively) characterized by a further flattening of the droplet and by the appearance of protrusions (indicated by arrows).

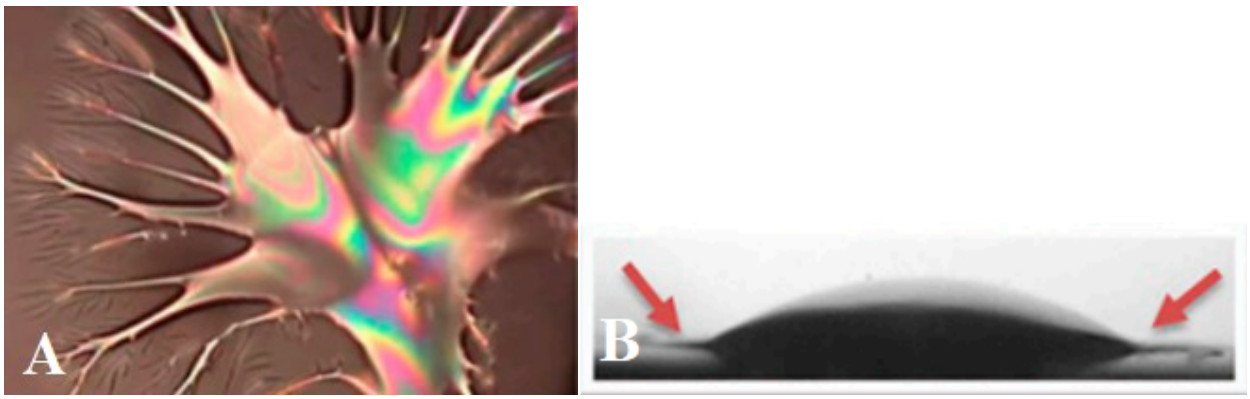

Figure 13. The explosive instability (A) and two fluid jets moving on substrate (B)

Figure 14 shows a sequence of images relating to the explosion on an iron-doped substrate in which it was observed a slower ejection of single jets of fluid (A), ejection of a great number of thin jets (B), large jets (C) and protrusion of large areas combined with jets ejection (D).

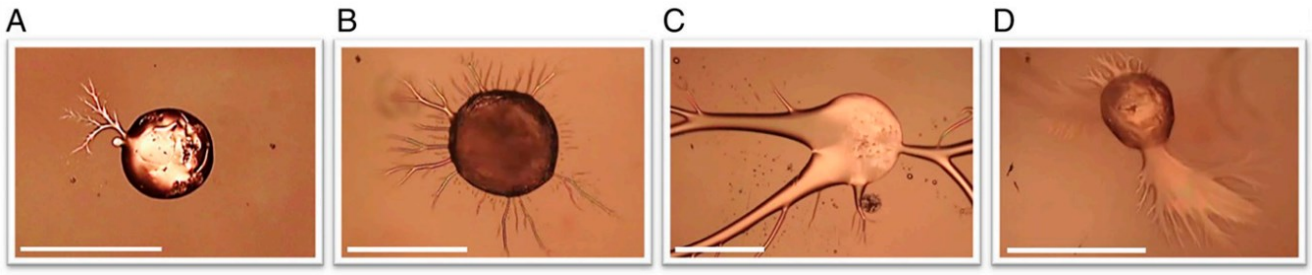

Figure 14. Gallery of explosions showing the initial stage of the phenomenon developing within the first tens of milliseconds for different droplets on iron-doped LN substrates (A–D)

The onset of instability occurs with different morphologies, as shown in Fig. 14. The different initial stages of the instability might be due to various factors, including differences in LN substrates, in droplets average diameter, and in cooling rates and variations in the instability temperature.

The role of electrostatics in this phenomenon is indicated by the fact that the instability here described crucially depends on the presence of the LN substrate. Sessile RM734 droplets are stable while cooling in the NF phase on other solid surfaces, including bare glass, Teflon, and glass coated with various polymers. The instability appears identical on the two sides of the LN substrate, indicating that the sign of the charges of the LN surface that contacts the LC droplet is irrelevant. This finding suggests that solubilized ions are not relevant to the instability, which is likely entirely due to LC polarization.

Since the liquid crystal is not a conductor, the observed shape instability occurs in the absence of free charges but with the requisite charging within the droplet arising from the intrinsic polarization of the ferroelectric LC via its contact with the ferroelectric substrate. The LN crystal has finite size, so its pyroelectric charging produces a fringing electric field E_f external to the crystal, as sketched in figure 15-A. The fringing field is a fraction f of the internal field $\sigma_{LN} / \varepsilon_0$, with $f \approx 10^{-3}$ depending on the crystal finite size and in the region of interest is largely in the vertical direction. The fringing field due to the finite size of the LN (figure 15-A) combined with the interfacial coupling produces an induced polarization of the ferroelectric droplet along z, which shields the field (Figure 15-B; side view). This polarization changes the surrounding field of the droplet which acquires a radial component (dashed blue arrows in figure 15-B; side and top view), which determines the elongation and movement of the jet in correspondence with the instability (figure 15-C). Figure 15-D is an illustration of a possible configuration leading to the local accumulation of charges at the edge of the drop and in figure 15-E we have that the instability is produced by the Coulomb force (F_c) overcoming the surface tension (F_s) and forms an area (S) smaller than the size of the drop. As this condition is met, the instability turns to an explosive runaway process since the flow of the liquid ferroelectric in

the nascent jet induces orientational order of the nematic director along the jet direction, which transports the polarization charge to its tip, in turn increasing the electrostatic repulsion [3].

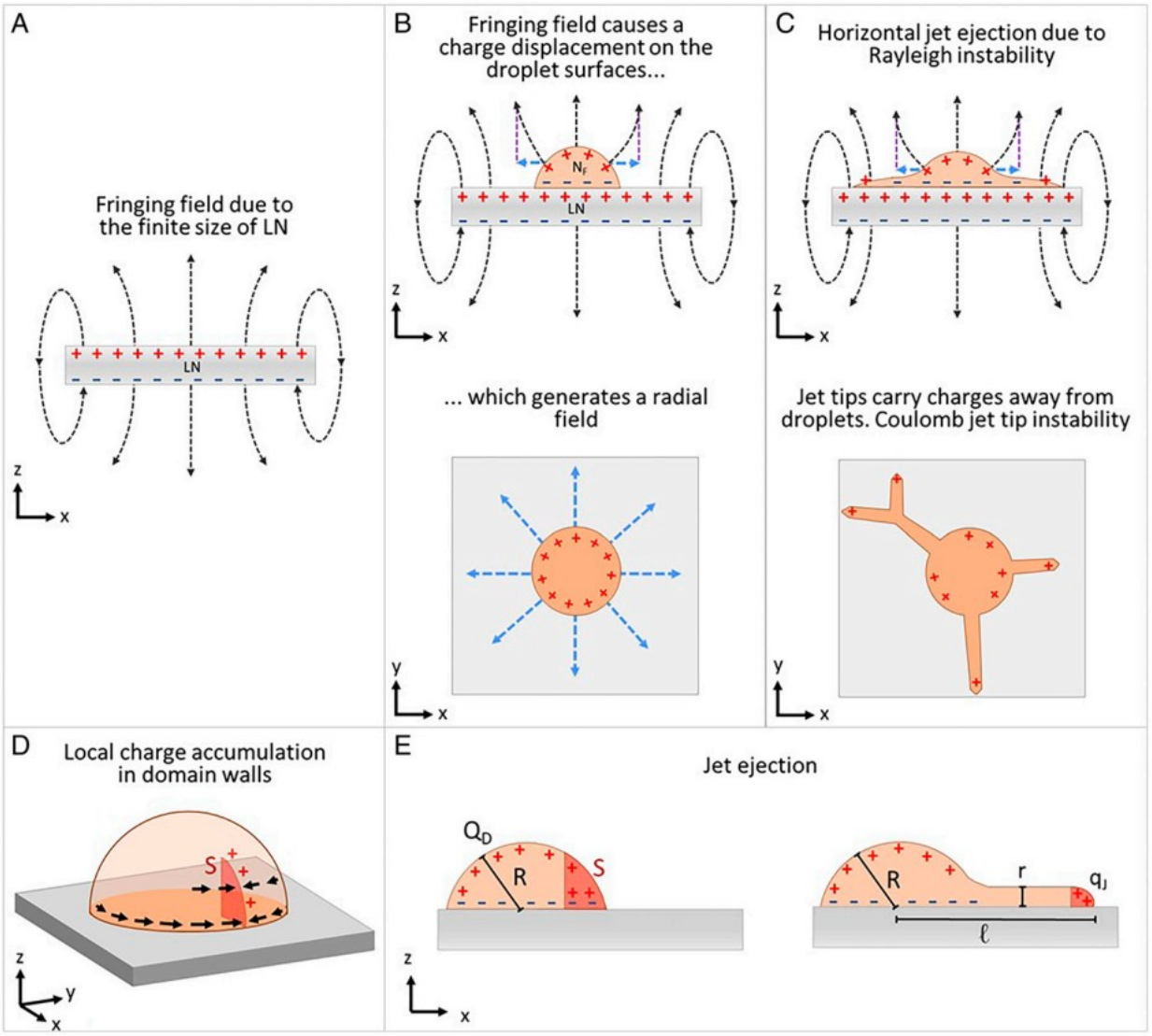

Figure 15. Sketch showing the steps leading to droplet instability.

The abrupt decrease of the contact angle observed in [3] as the droplet enters the NF phase, is an indication that a decrease of the surface tension precedes the instability. This variation of the surface tension has been ascribed to the Coulomb repulsion between the polarization charges deposited on the droplet surfaces as it enters the NF phase, aimed at cancelling the internal field. It is thus a very relevant ingredient of the observed instability and of the way in which the polarization of the two materials couple. Since such a novel combination of ferroelectric solids with ferroelectric liquids has never been observed before and since it can have important applications in several fields, it is interesting to characterize and understand it in more details. One step in this direction is the systematic study of how the wettability of RM734 sessile droplets varies with temperature.

The experiments described in the following chapter, aim at characterizing the mentioned surface tension variation in LN substrates with different doping levels and different values of the reduction factor R. As a comparison, measurements were also performed on bare glass.

CHAPTER 2

2.1 Experimental procedure

The following chapter describes the various phases of the preparation of the materials used, the set-up used for the measurements and the various tests carried out.

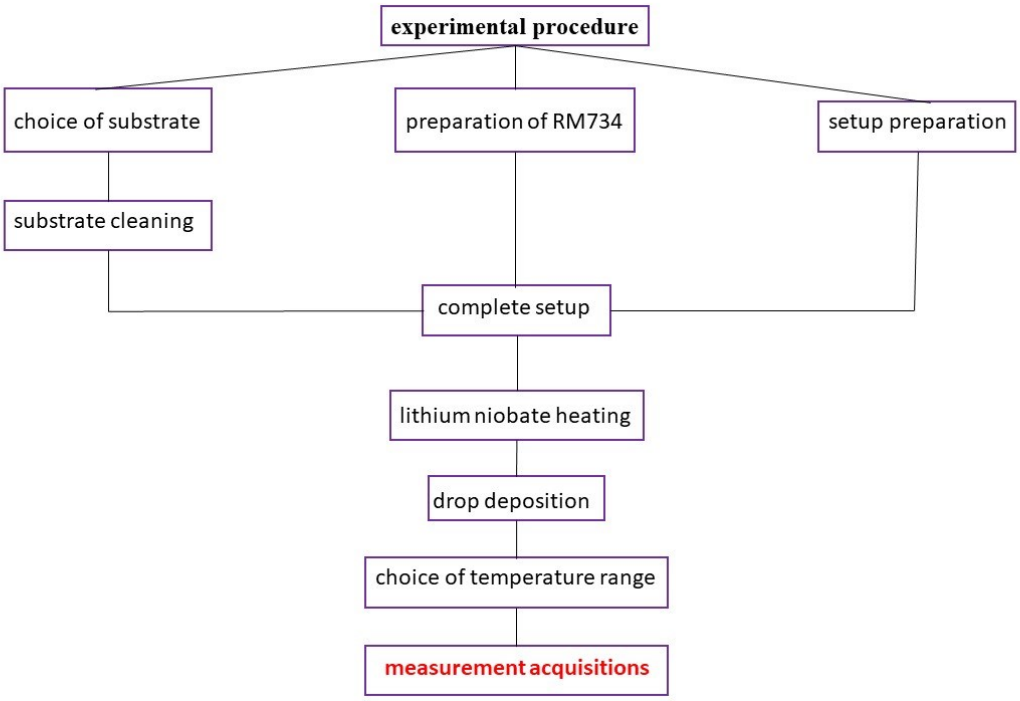

Figure 16. Block-scheme of experimental procedure

All the experiments were carried out in the laboratories of optics of the Department SIMAU at Università Politecnica delle Marche. The first step is to prepare the setup in which the experiments will be performed. They will be performed on the optical bench and it's very important to have an excellent alignment between all the components and the CCD camera. A representation of the setup is shown in the following paragraphs. The RM734 sample is deposited on the substrate (glass or lithium niobate), which in turn is placed on a plate used for thermalization, as in figure 17. The exact position of the substrate with the drop is on a cavity in the plate. The optical alignment for image acquisition was performed by means of a red low power laser which was then replaced with a white light LED, more suitable for obtaining good images. A green laser has been used for seeing the various phase transitions of the liquid crystal as a function of temperature. For the acquisition of the images and videos a CCD was used for the lateral view of the drop and a reflex camera for the top view of the drop. Both cameras are controlled by the computer, in this way the risks of destabilizing the system have been avoided and everything remains aligned. Figure 18 shows a scheme of the setup used to align all the components, from the light source to the camera to obtain focused images of the drop..A converging lens was used between the red laser and the drop in order to have the entire profile

of the drop illuminated by the laser. Then, two converging lenses were used between the drop and the CCD to form the image in the camera and keep the magnification fixed.

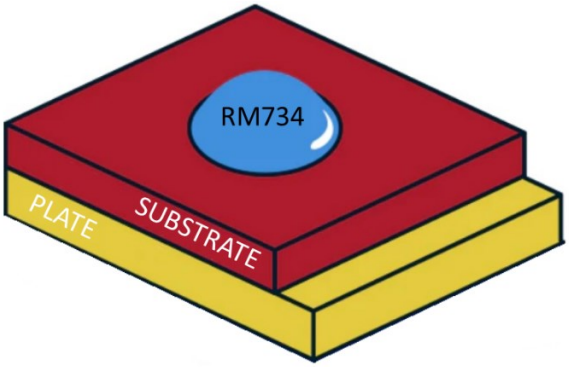

Figure 17. Plate, substrate and liquid crystal arrangement

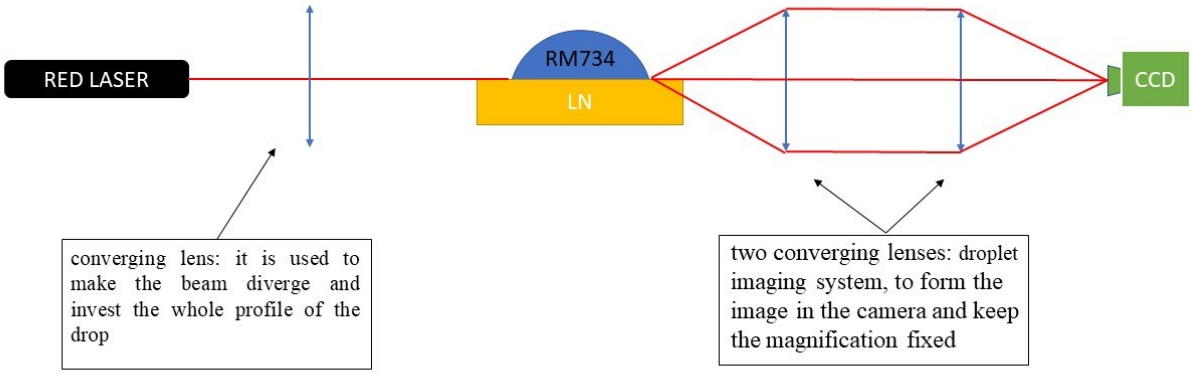

Figure 18. Alignment of the components in the set-up with red laser

Figure 19 shows the setup used for the measurements; a white light LED was used as the light source. This light has been passed through a converging lens and once passed through the drop, the light passes through two converging lenses and reaches the CCD in order to capture and obtain an image of the lateral profile of the drop. As for the use of the green laser, since it can affect the liquid crystal orientation it has been used with the minimum intensity (about 0.1 W/cm^2) and for short periods of time (through the use of a shutter we can interrupt the flow of light directed towards the drop), with a beam waist 1mm, way larger than the droplet size. By opening the shutter, the green light beam reaches the drop and illuminates it from below. Thanks to it, we can see, based on how the light

spreads in the drop, the phase in which the liquid crystal under examination is found. Video and photos of the drop from above were taken by a Canon D750 reflex camera.

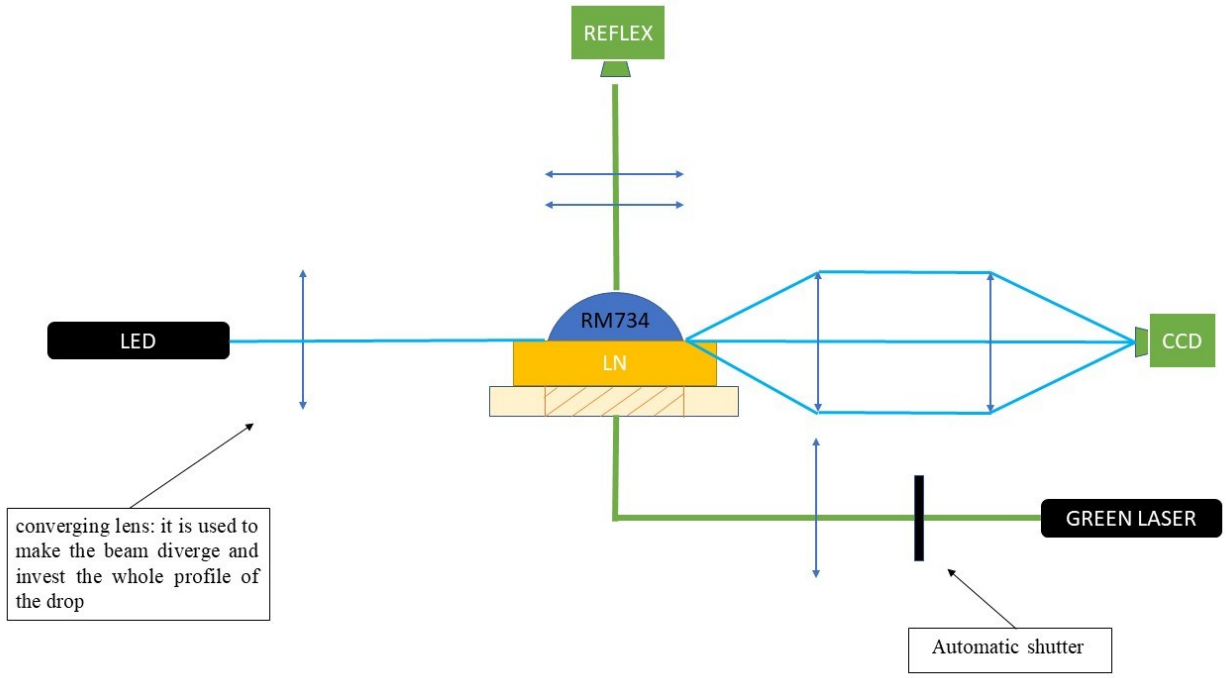

Figure 19. Block diagram of the set up used.

2.2 SUBSTRATES

Once the optical bench has been prepared with the setup to be used, the type of substrate with which to carry out the experiment is chosen. The first test was carried out on bare glass and the second on a commercial undoped LN substrate with a thickness of 900 µm. All other experiments were performed on iron-doped lithium niobate substrates. Figure 20 shows the various iron doped substrates used.

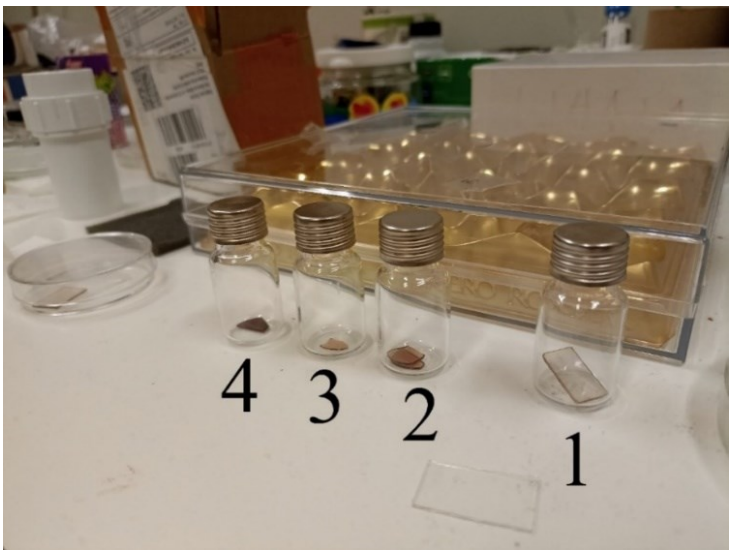

Figure 20. Lithium Niobate substrates

All substrates shown in the image are all doped with the same amount of iron (0.1%) except one. Substrate number 3 contains 1% iron. Some crystals are doped not in the bulk, but only in a thin surface layer and in this case the doping is called diffuse. Specifically, we have:

- Substrate number 1 is defined as diffusely doped as the iron is present in the 30-micron layer on one of the 2 faces. The side where this layer of iron is present will be indicated with the letter B while the other side will be indicated with the letter A.
- Substrates number 2, 3, 4 are all volume doped, with different reduction factor (R).
- Substrate number 3 has a thickness of 900 μm and R=0.03.
- Substrate number 2 has a thickness of 500 μm and R=0.001.
- Substrate number 4 has thickness of 850 μm and R=1.05.

Once the substrate has been chosen, it must be cleaned to avoid having contamination from other experiments. The substrate is first cleaned with acetone and then with ethanol, for a more thorough cleaning it is placed inside a small baker filled with ethanol, which is then placed inside an ultrasonic cleaner for 2 minutes. Now we place on the heatable plate a thin (1mm thick) glass slide on which we place the substrate. The glass is tinted black around the edges to reduce scattering when light passes through it. The plate contains some resistive cartridges that are connected to a current generator which is controlled directly by the computer through the LabView SP1 2019 program. The same program also displays the temperature measured by a probed glued with conductive paste to the heatable plate.

In order to analyze the changes in RM734 wettability as a function of temperature, we started from the LC isotropic phase and cool down to the crystalline phase. To this purpose, before droplet deposition, the temperature of the substrate was slowly raised to 220°C. In these conditions, a small amount of RM734, which at room temperature is in the crystal phase, deposited on the lithium niobate crystal, immediately enters the isotropic phase and forms the drop that we are going to analyze. Our goal is to study the droplet contact angle in the different phases, by lowering the temperature until the electromechanical instability leading to explosion is eventually reached. The investigated temperature range is the same for all substrates, but different behavior of the ferroelectric liquid crystal has been observed. The cooling ramp was carried out by decreasing T of 5°C at a time and for each temperature reached an image was saved in the PC. The experiment can be considered concluded when the typical shape of the drop is completely lost, due to explosion events. An example of the typical images acquired during the experiments is shown in figure 21, in which it can be seen how the shape of the drop changes as a function of temperature. In these pictures we can see that at a temperature of 220°C, the liquid crystal is isotropic. At a temperature of 102°C it is noted that the drop becomes flattened with a slight variation of the contact angle with respect to the initial conditions. After a few seconds a jet of fluid which leads to the variation of the shape of the drop is observed (photo at T=95°C). Upon lowering the temperature futher, the typical shape of the drop is no longer distinguishable at T=90°C.

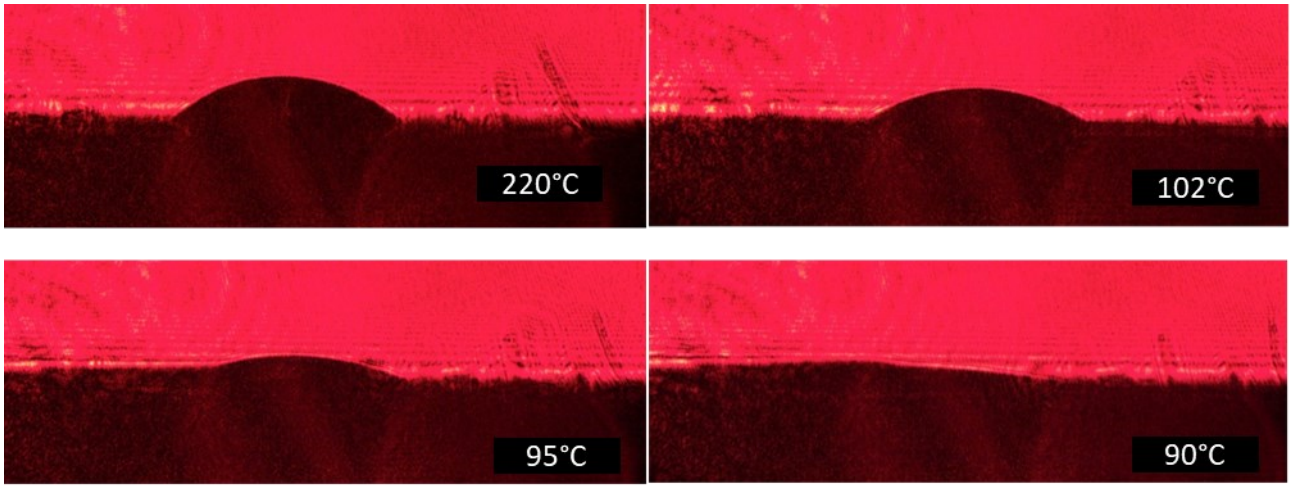

Figure 21. Contact angle and shape variation of the drop for different temperatures (side view)

2.3 CONCTACT ANGLE

Before going on with the description of the experiments, a brief introduction to the concept of contact angle is needed. Let us consider a certain amount of liquid in contact with a solid surface (figure 22). In most cases the liquid will not completely wet the solid but will take the shape of a drop with a well-defined contact angle. The value of the contact angle, indicated in Fig. 22 with θ_0, depends on the surface tensions between the phases involved.

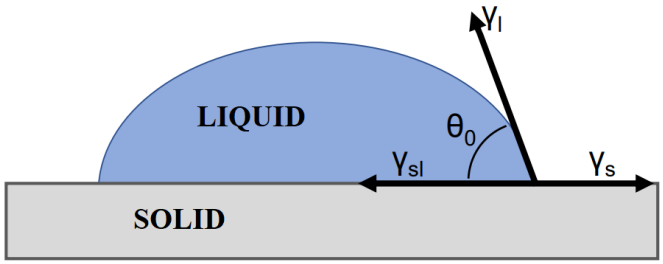

Figure 22. The value of the contact angle assumed by a drop of liquid on a surface.

In figure 22, it is shown the so called triple line, i.e. the ideal line that separates the three phases: solid, liquid and vapor. Three different surface tensions γ, will act on each infinitesimal section of this line, balancing each other in the equilibrium condition:

$$\gamma_{SV} - \gamma_{LS} - \gamma_{LV} \cos\theta_0 = 0$$

where SV, LV and LS mean solid-vapor, liquid-vapor and liquid-solid, respectively. The above equation is known as the Young Equation. From this equation, the value of the contact angle can be obtained as a function of the surface energies:

$$\cos\theta_0 = \frac{\gamma_{SV} - \gamma_{LS}}{\gamma_{LV}}$$

Therefore, the contact angle is a useful index to characterize the wettability of a surface (figure 23). In general, if a liquid on a surface gives rise to a contact angle lower than 90° it is stated that the surface is wettable by the liquid, otherwise it is said not wettable. If the test liquid is water, the surface is said hydrophilic in case of high wettability and hydrophobic in case of low wettability.

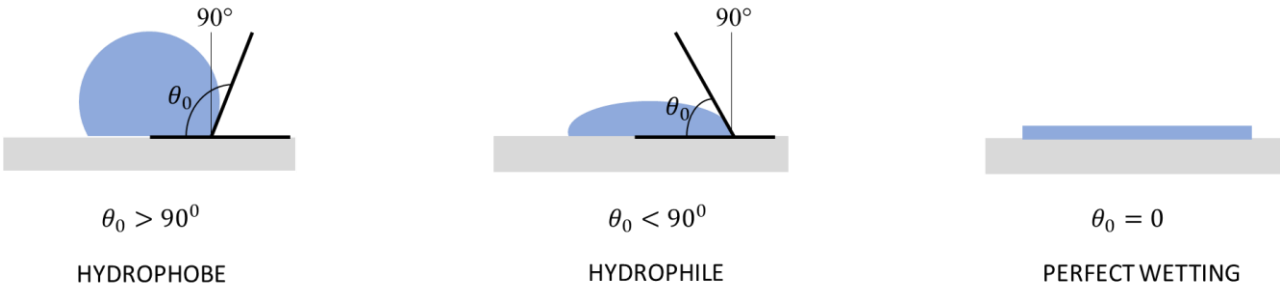

Figure 23. The contact angle is an indication of the wettability of a surface.

CHAPTER 3

3. Analysis

This chapter deals with the analysis of measurements made in the laboratory: we will explain how we evaluated the contact angle between the drop of RM734 and the lithium niobate substrate starting from the raw images, obtained as described in Chapter 2.

3.1 PROCEDURE FOR ANALYSIS OF MEASUREMENTS

All the steps concerning the analysis of the images obtained from the laboratory tests are shown in the diagram in figure 24:

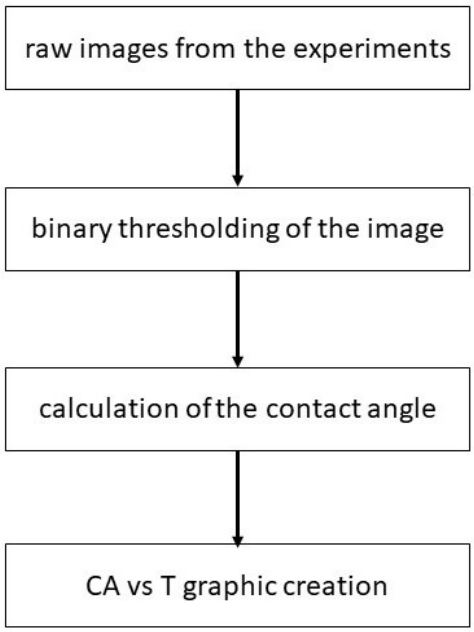

Figure 24. Image analysis phase block diagram

The droplets contact angles as a function of temperature, were obtained from the images acquired during the cooling ramps. Using the three different software listed below, we passed from the simple image of the lateral profile of the drop to the final graph where the contact angle and the temperature are related.

3.1.1 Binary thresholding of the images (ImageJ)

The first software used is ImageJ, a software for digital processing of images. In the program we import all images related to a single experiment as image sequence (each image corresponds to a certain temperature). First, we need to filter the image using the “gaussian blur” function. The "gaussian blur" function blurs the image by performing the convolution by means of a Gaussian square kernel. Secondly, we use the functions "split channel", where the images are split into the 3 colors of the RGB model and we choose the color that best distinguishes the drop profile, then “threshold”. The “threshold function” allows us to interactively set the smallest and largest threshold value, segmenting the image into the features of interest and the background. Pixels with brightness value greater than or equal to the lowest threshold and lower than or equal to the highest threshold, are displayed in red. Alternatively, to achieve the same result, one can execute the "convert to mask" function. The images obtained must be saved as an image sequence in the PNG format. The saved images must undergo a last step in which a fixed baseline is created so that we have the drop always in the same position because small undesirable movements of the plate may have occurred during measurements. We do this through the "registration" command. The sequence of images obtained is saved in AVI format. As an example, figure 25 reports an image obtained from the CCD on the left and the corresponding image processed with ImageJ on the right.

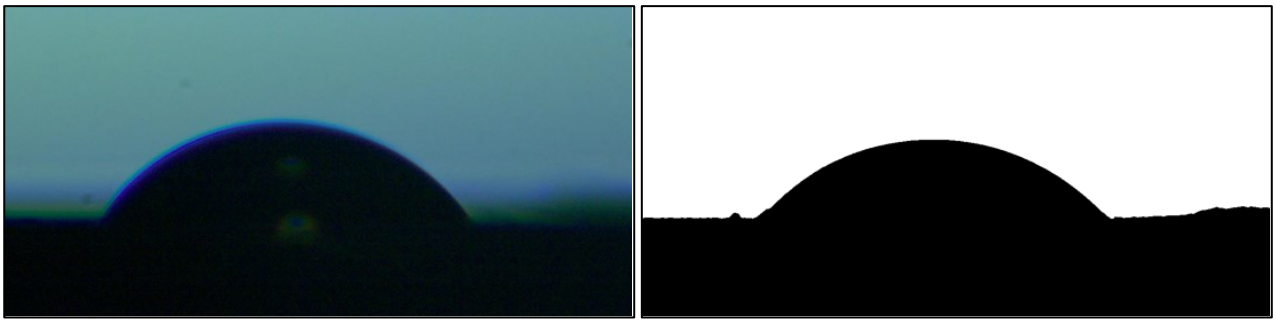

Figure 25. Process result obtained with ImageJ

3.1.2 Calculation of the contact angle (Ossila software)

The second software used is Ossila, which allows us to determine the contact angle of the drop. In our case we measure the contact angle of several images belonging to the same experiment and for this reason a sequence of images saved in AVI format was previously created with ImageJ. We import the file with the image sequences to Ossila, which are loaded immediately and appear on the monitor. With a red rectangle we define the area where we want the measurement to be made, the software recognizes the shape of the drop and will start calculating the left and right contact angle for each image. It is important to calculate both the left and right contact angle of the drop because during the experiments instability phenomena might occur which lead to the emissions of fluid jets in a random position, creating an asymmetrical contact angle. The results are shown simultaneously with the scrolling images. Figure 26 shows the Ossila screen in which the processed photos have been loaded. Here the contact angles are calculated and in the upper right corner it is possible to see a graph in which the angle values are reported (the red dots correspond to the measurements of the right angle while the blue dots correspond to the measurements of the left angle). Edge detection of the droplet was combined with a polynomial fitting method to calculate the contact angle in each frame of the

video and the graph with the results are shown in figure 27. Once the measurement is finished, we save the file with the .CSV extension.

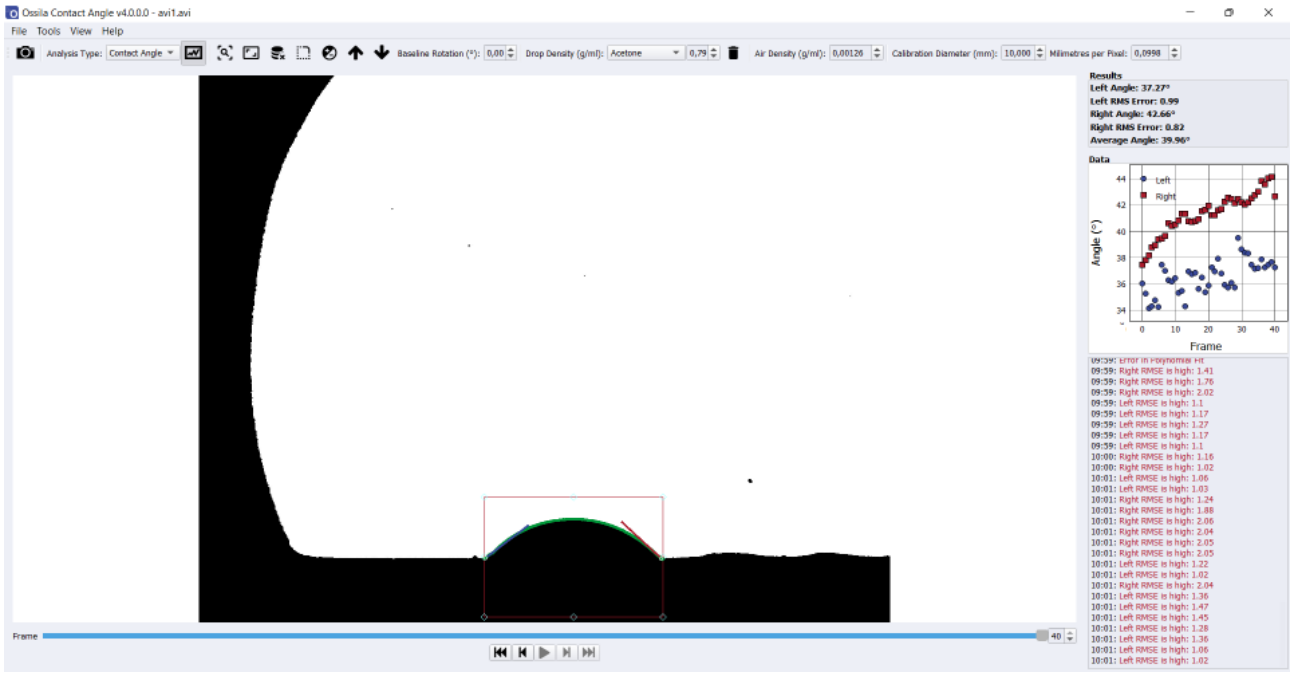

Figure 26. Screenshot of the Ossila software to carry out a contact angle measurement

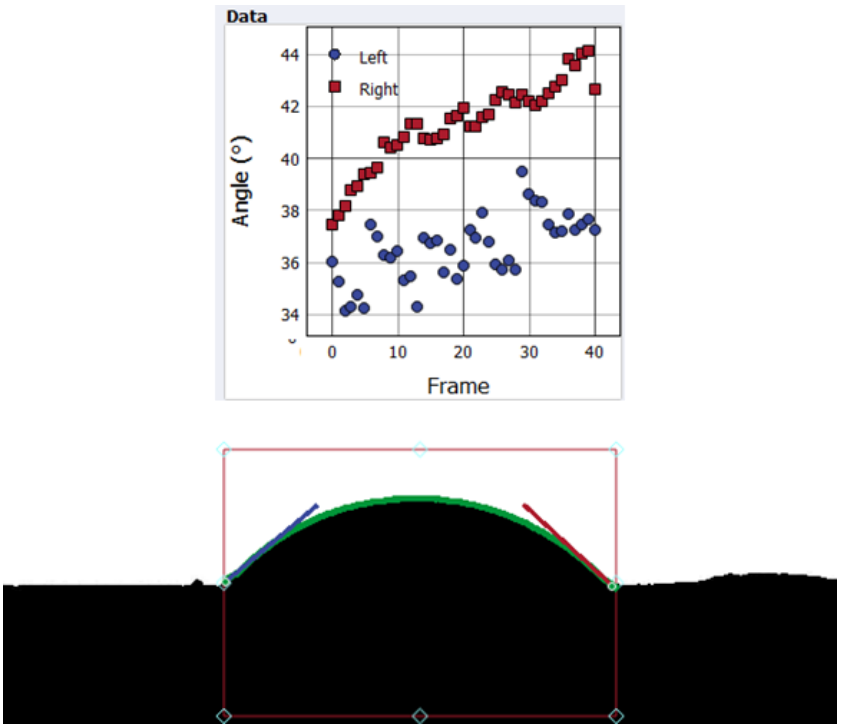

Figure 27. Edge detection of the drop and graph with result of the contact angle measurements

3.1.3 Creation of the contact angle vs Temperature (CA vs T) graphs (Visual Code Studio)

The last step was done through Visual Studio Code, which is a source code editor; in our case the Python programming language was used and through the formulation of a code the values of the contact angles (left and right) were reported as a function of temperatures. In figure 28 we can see an example of the final graph obtained. The background is divided into three different colors used to distinguish the different phases of RM734 (for the transition temperatures we referred to [9]). The isotropic phase is shown in blue, the nematic phase in gray and the ferroelectric nematic phase in yellow. The graph legend shows the symbols belonging to the graph and in particular the blue dots indicate the trend of the left contact angle while the red dots indicate the trend of the right contact angle. The black dots represent the contact angle obtained by averaging the left and right angles. The vertical dashed lines in the yellow region of the graph, mark explosion events. The red dotted line indicates the temperature corresponding to a total loss of the droplet shape. The distinction we made between the emission of the first jet (green dotted line in Fig.28) and the explosions (blue and black dotted lines) is based on the fact that in the first case there is only the presence of jets of fluid in precise areas from the drop while in the second case they are phenomena that concern the whole drop and it is an event that changes the morphology of the surface of the drop.

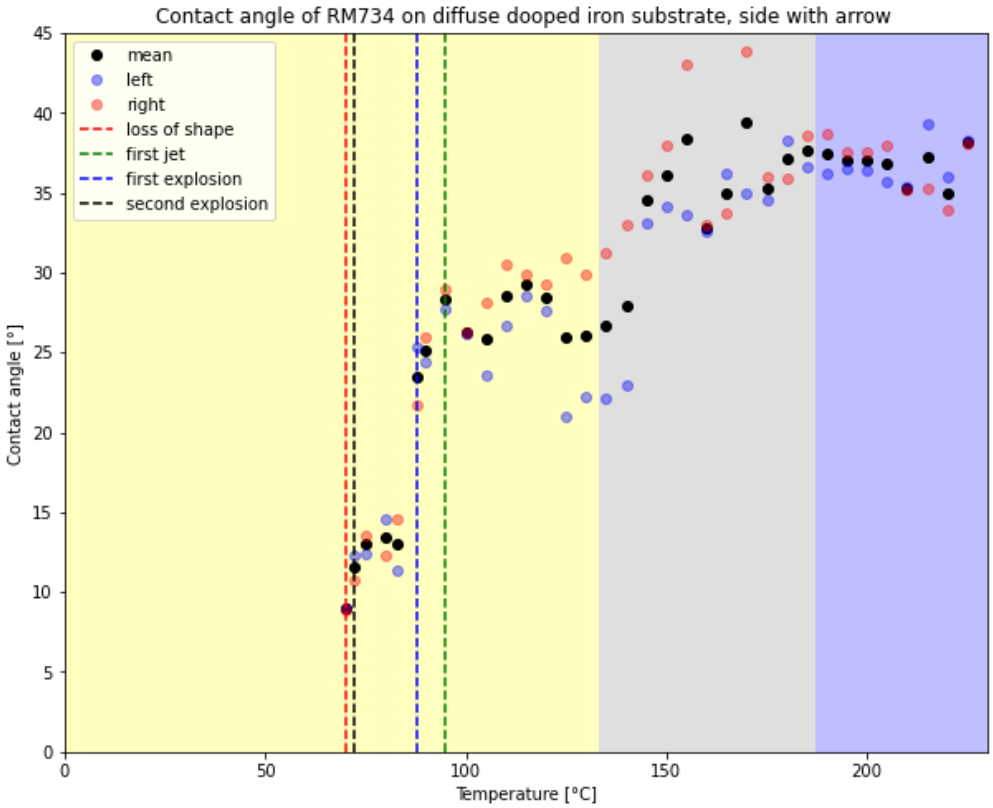

Figure 28. Final graphic example CA vs T

3.2 EXPERIMENTAL ERROR

The values obtained are affected by error being obtained from an experimental procedure. The main error is related to the one caused by the operator during the interpolation of the line with the profile of the drop using Ossila to calculate the contact angle. Through various tests by slightly varying the inclination of the straight line which interpolates the profile of the drop, it has been estimated how much the measured contact angle can vary. From the average of the various tests, 3° corresponds to the maximum error that can be made in the interpolation phase. Beyond 3°/ 4° the operator can see that the straight line does not intersect the drop profile correctly. Figure 29 shows an example.

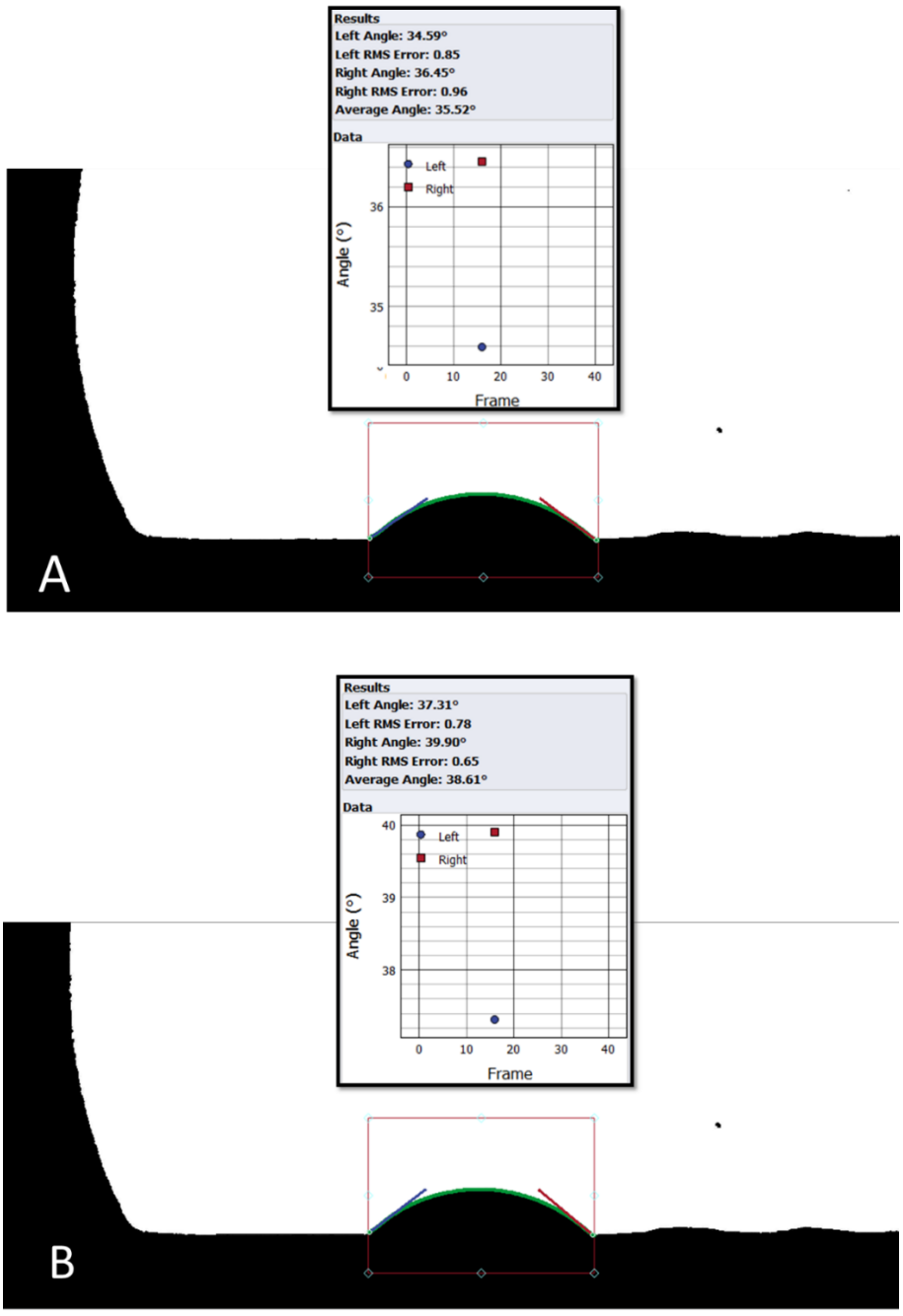

Figure 29. Example error due to the interpolation between the straight line and the profile of the drop

Figure 29 shows two cases in which the slope of the interpolating line varies slightly in the same frame and consequently we have different values. The ideal case is when the straight line is as tangent as possible to a point of the drop which corresponds to the case shown in figure 29-A, by slightly changing the inclination we can observe that the straight line is always tangent to the edge of the drop outlined by Ossila but the value is different as we can see in figure 29-B. Between the two tests on the same frame, as in the other tests carried out, there is an average contact angle which varies by approximately 3°.

The results will show the graphs with the contact angle averaged between the left and right angles in which the error on the single measurement and the difference between the left and right angle are both taken into account, as shown in the following formula:

$$E_{TOT} = \sqrt{((err_{\theta})^2 + \left(0.5 * (\theta_{DX} - \theta_{SX})\right)^2)}$$

CHAPTER 4

4. Results

This chapter will show the results of the experiments performed on the different types of substrates used. The variation of the contact angle with temperature will be represented by graphs. The trend of the left and right angle values is the same in most of the experiments but in some cases is different as on bare glass substrate represented in figure 30:

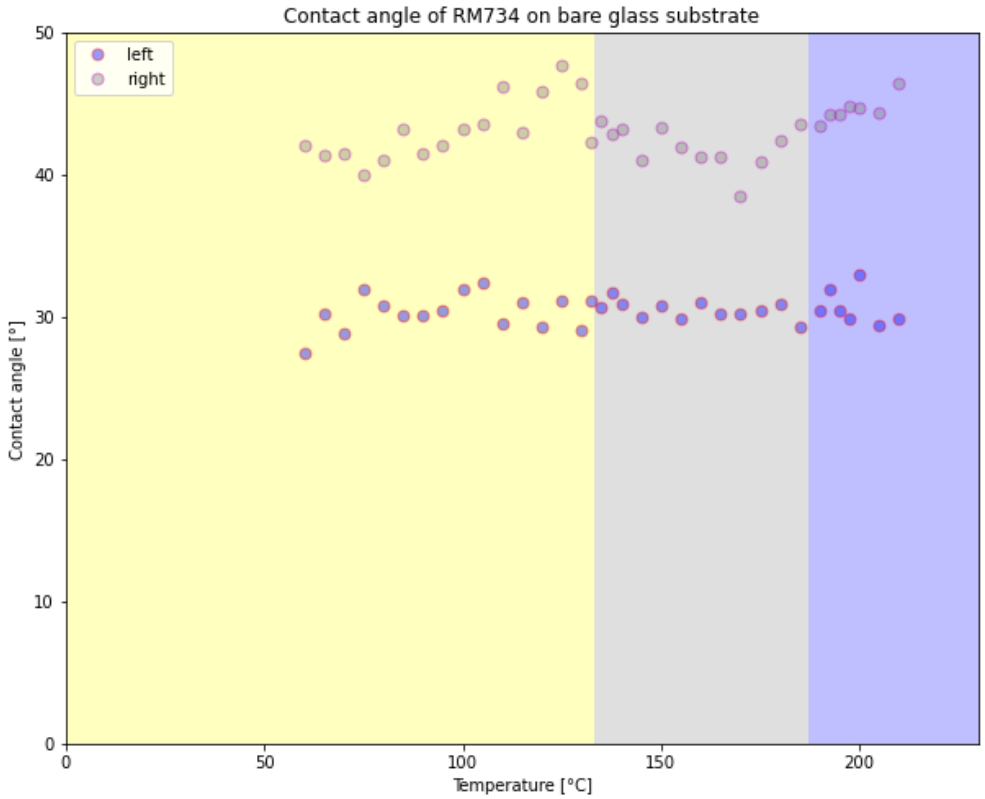

Figure 30. Different left and right contact angle trend on bare glass substrate

This graph includes 2 curves: the curve with the blue dots represents the left contact angle values, the curve with the red dots represents the right contact. The large difference observed between the two contact angles is probably due to the combination of the magnitude of the drop and the procedure for deposition of the drop on the substrate. In fact, the size of the drop can be decisive since the larger the drop, the more likely it is to be asymmetrical. Also the drop deposition procedure can cause asymmetry due to the precision of the operator during this phase.

All the experiments have been carried out starting from a temperature of 210°C/220°C, corresponding to the RM734 isotropic phase. The isotropic phase is indicated by the blue band and the transition from isotropic to nematic occurs at a temperature of 187°C. From 187°C to 133°C the LC is in the nematic phase, which is indicated with the gray band. The ferroelectric nematic phase, that begins at

T = 133°C, is indicated with the yellow band. The results will be shown on graphs where the average between the left and right angle is represented. The background with the three different colors always represents the different temperature-related phase transitions. As discussed at the end of chapter 3, information is added regarding two observed phenomena which are jets and explosions:

- Jet: limited ejection of material from the liquid crystal drop in which the shape of the drop is preserved.
- Explosion: phenomenon in which there is a greater amount of material expelled from the liquid crystal drop compared to the jet. In this case, after the event, the typical final shape of the drop is different from the previous shape in terms of size or shape.

They are represented with different colors, usually green indicates the jet while red indicates the explosion and are indicated in the legend of each graph. The graphs also include the errors that were calculated for each experiment as indicated in chapter 3 section 3.2.

4.1 BARE GLASS SUBSTRATE

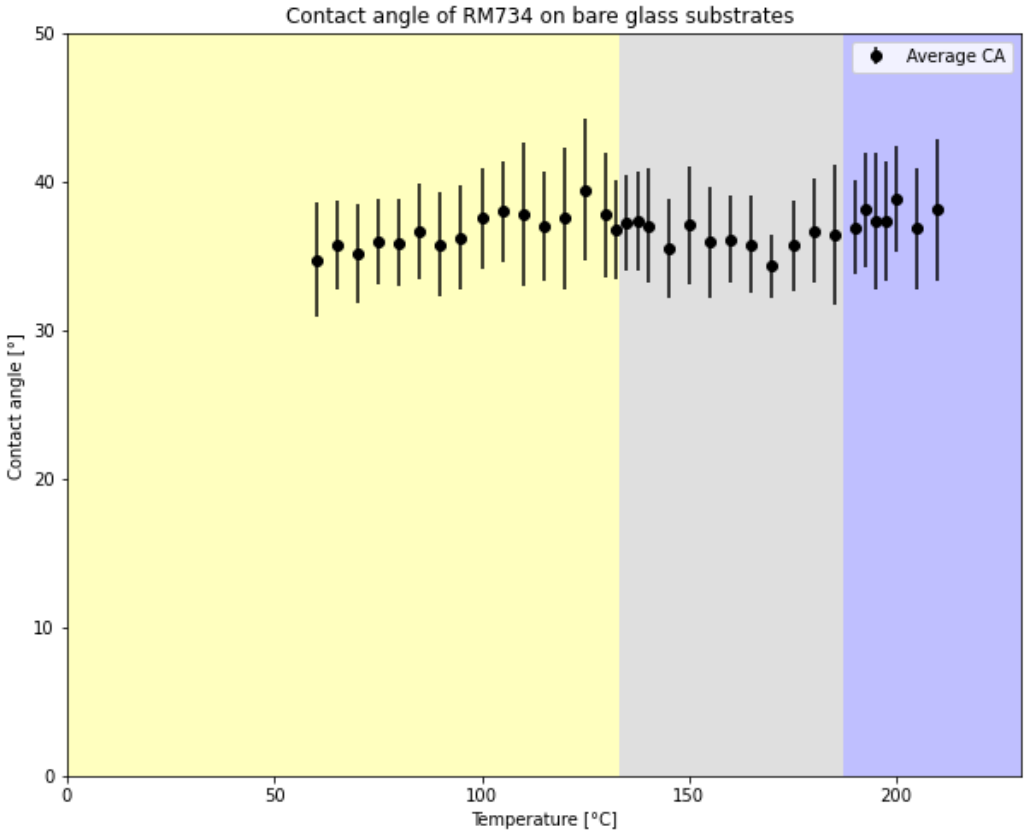

Figure 31. CA vs T graph of RM734 on bare glass substrate

The experiment on bare glass starts from a temperature of 210°C. The average contact angle ranges from 35° to 38°. At a temperature T = 60°C the drop begins to crystallize without any event of jet

ejection or explosion, as expected due to the absence of any polarization of the substrate. Figure 30 shows that the RM734 contact angle is approximately independent on T, in the explored temperature range, which suggests that the LC surface tension at the interfaces with air and with glass do not vary much. The lateral profile of the drop at T = 60°C is shown in Fig. 32.

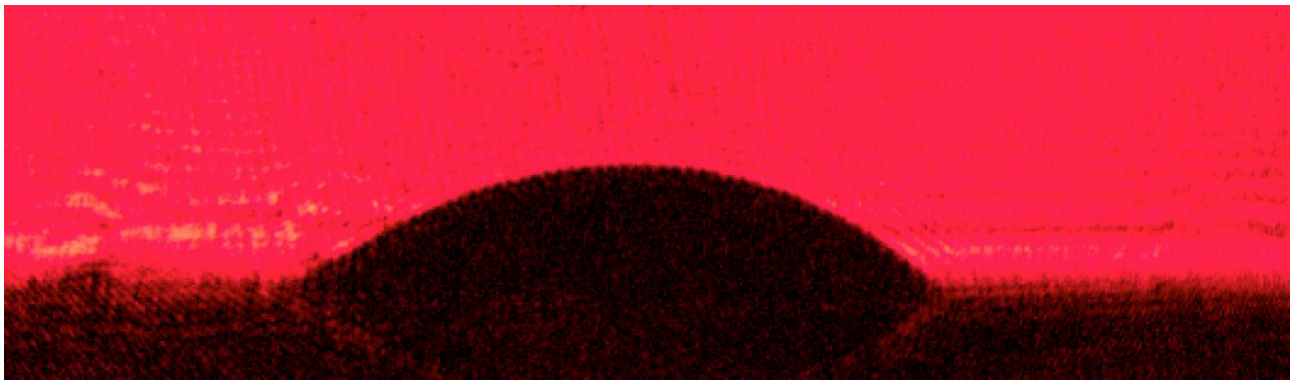

Figure 32. Droplet side profile of RM734 on simple glass substrate at the temperature of 60°C

4.2 COMMERCIAL UNDOPED LN SUBSTRATE

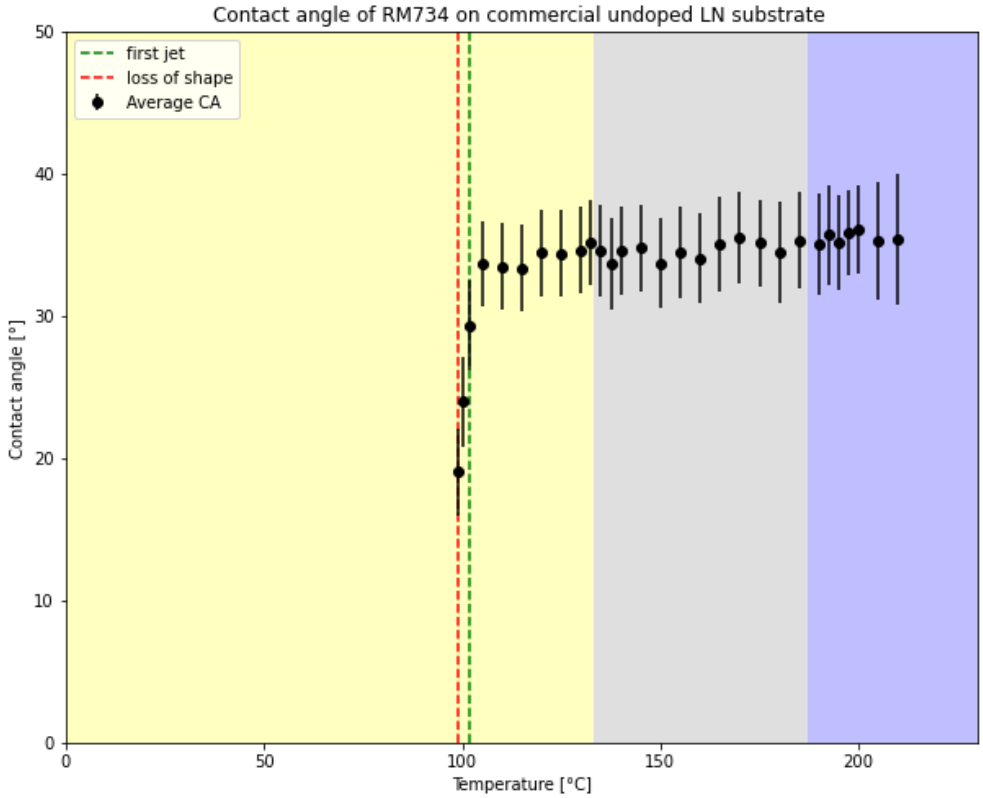

Figure 33. CA vs T graph of RM734 on commercial undoped LN substrate

In this case, the experiment starts at T = 210°C and stops at T =99°C. When T reached 102°C a sudden decrease of the contact angle was observed and the ejection of a fluid jet occurred. The average contact angle is 34°. After the ejection of the first jet, we observe a change in the contact angle value due to the deformation created by the jet itself. At T =99°C the droplet undergoes a violent explosion and completely loses its dome shape. This is visible in Fig. 34, where the continuous expansion of the fluid from the area where the drop was present is shown.

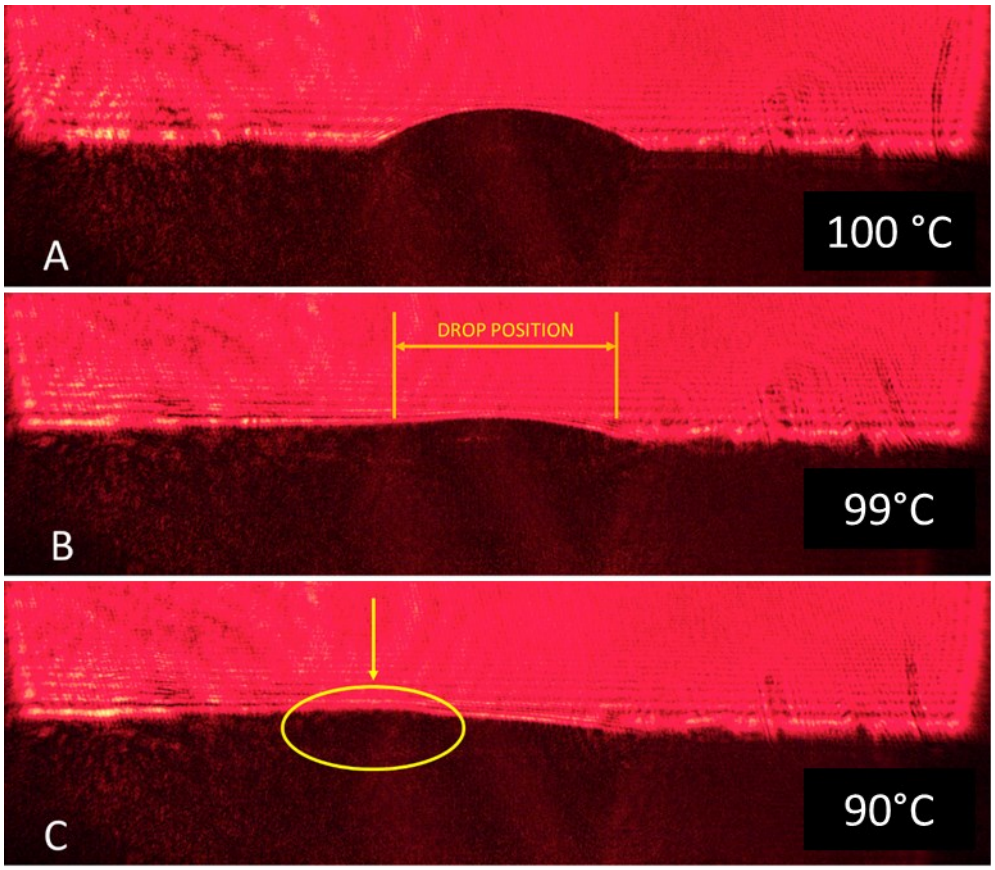

Figure 34. Lateral expansion of the fluid after the explosion.

Figure 34-A shows the RM734 drop at T = 100°C exhibiting its conventional dome shape. In figure 34-B the drop, marked by a yellow segment, is still partially visible after the explosion, while in figure 34-C, the fluid that expands on the left of what remains of the drop is visible in the marked area.

4.3 Fe:$LiNbO_3$ (DIFFUSED DOPED) SUBSTRATE (A)

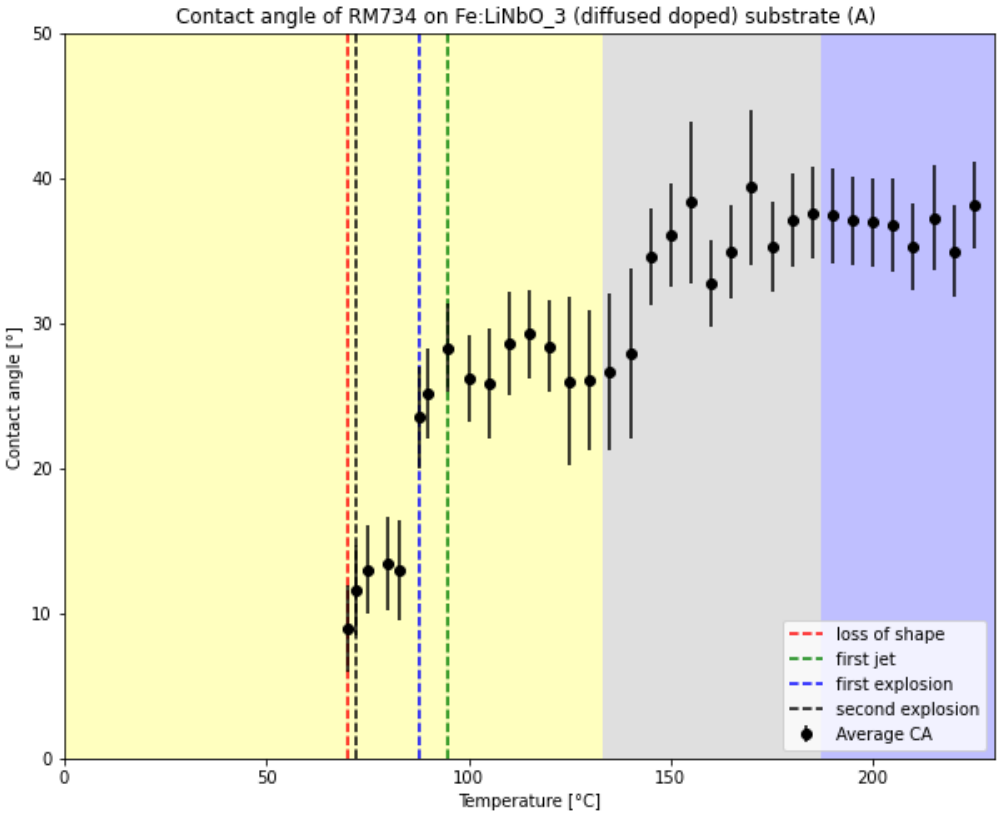

Figure 35. CA vs T graph of RM734 on Fe:$LiNbO_3$ (diffused doped) substrate (A)

The Fe:$LiNBO_3$ diffused doped substrate (A) is the one in which the greatest changes in the contact angle were recorded. In this case there was a different behavior compared to the other substrates as more instability events with jet ejection occurred at different temperatures followed by explosions which consequently modified the shape of the drop. The first jet occurred at T = 95°C, soon after there was a second larger jet which led to the first explosion at a temperature of 88°C. Further lowering the temperature, a second and sudden explosion (72°C) took place which immediately after, led to the loss of the drop shape (70°C). Until T = 65°C a slow but continuous flow of material is observed from what was the mother drop.

4.4 Fe:$LiNbO_3$ (DIFFUSED DOPED) SUBSTRATE (B)

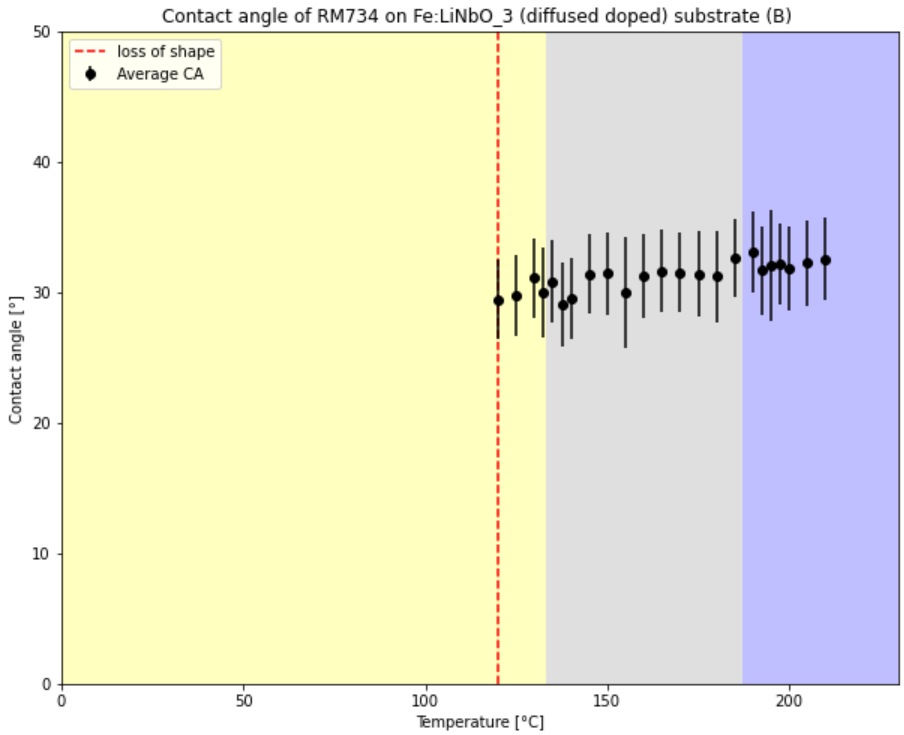

Figure 36. CA vs T graph of RM734 on Fe:$LiNbO_3$ (diffused doped) substrate (B)

The experiment on this substrate, starts at T = 210°C. In general, during the entire duration of the experiment, no particular phenomena occurred and the drop didn't undergo large deformations until the onset of the instability, which led to the sudden explosion at T = 120°C. During the cooling ramp a slight decreasing trend is noted, with an average contact angle of 30°.

4.5 Fe:$LiNbO_3$ (R=0.001) SUBSTRATE

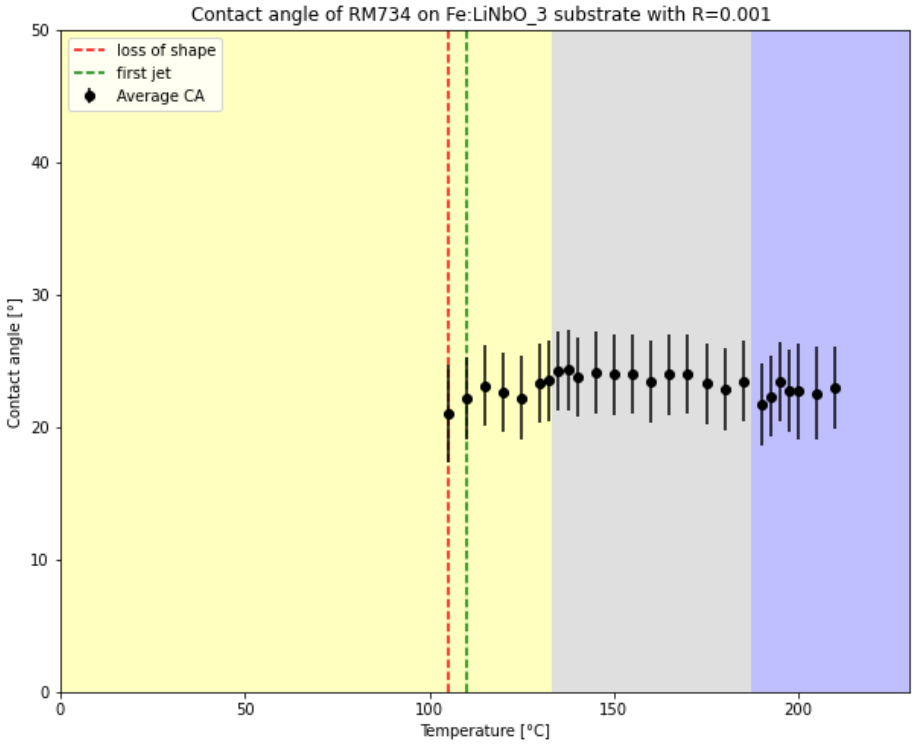

Figure 37. CA vs T graph of RM734 on Fe:$LiNbO_3$ (R=0.001) substrate

The experiment on the Fe:$LiNbO_3$ substrate with a reduction factor R = 0.001 starts from a temperature of 210°C while the instability takes place at T = 105°C (green dashed line). From T = 110°C a variation of the shape on the right side of the profile of the drop is observed, which involves a decrease in the value of the right contact angle. Following the explosion at 105°C, the drop shape is no longer distinguishable and a small and constant expansion of the fluid on the substrate is observed until T = 90°C. Figure 38 shows the drop before (A) and after (B) the explosion. The fluid expansion over the substrate is marked with a yellow arrow (Fig. 38-B).

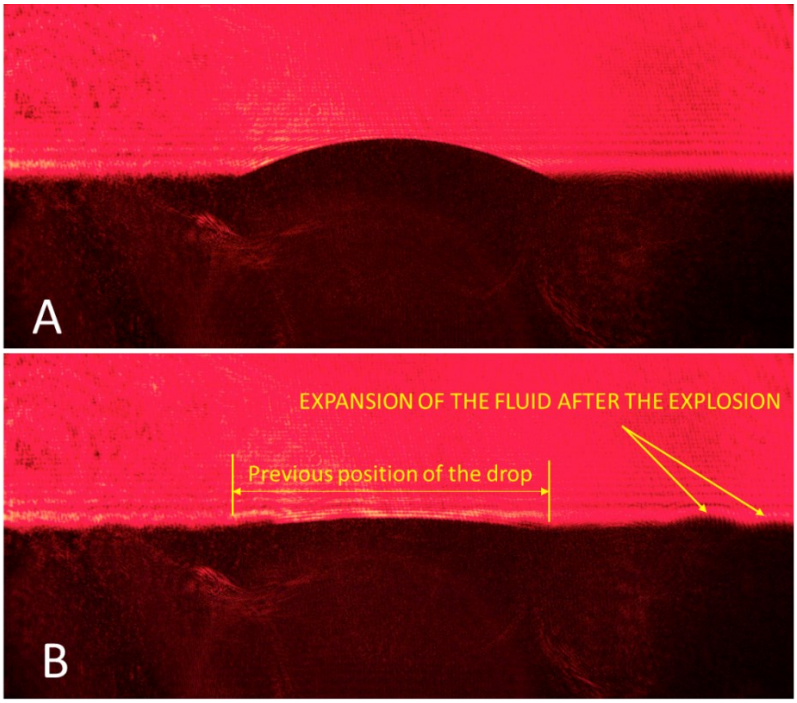

Figure 38. Expansion of the fluid after the explosion on Fe:$LiNbO_3$ (R=0.001) substrate

4.6 Fe:$LiNBO_3$ (R=0.03) SUBSTRATE

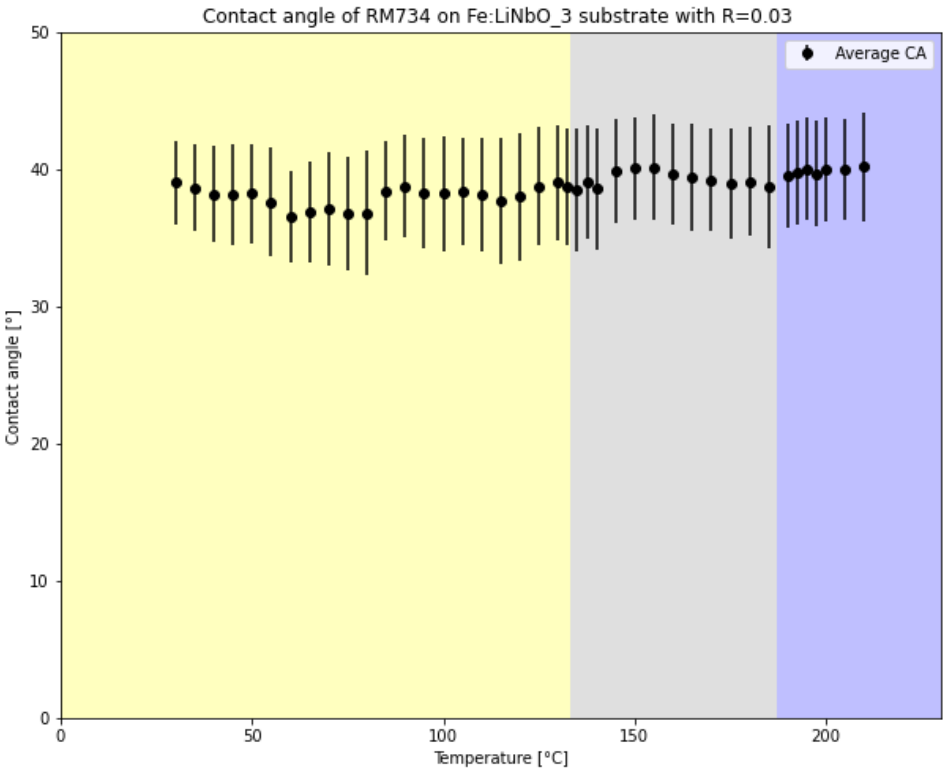

Figure 39. CA vs T graph of RM734 on Fe:$LiNbO_3$ (R=0.03) substrate

The behavior of the RM734 droplets on this substrate is quite peculiar and unexpected. Indeed, this is the only LN substrate over which we did not observe any instability event. Starting from T = 205°C and throughout the whole cooling range, we observed a condition of stability ending with the drop crystallization. More information will be included in the discussions in chapter five.

4.7 Fe:$LiNBO_3$ (R=1.05) SUBSTRATE

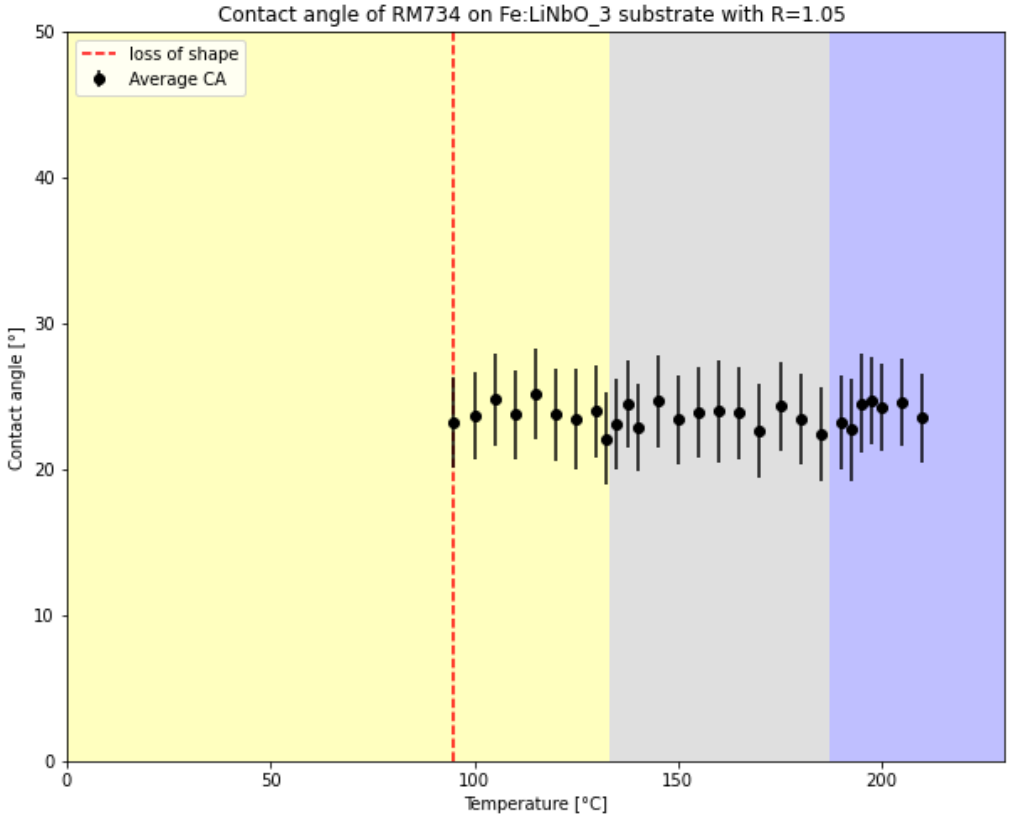

Figure 40. CA vs T graph of RM734 on Fe:$LiNbO_3$ (R=1.05) substrate

From the starting temperature of 210°C, both left and right contact angles do not vary much and remain on average around 24°. From both the data in the graph and the photos of the side profile of the drop it can be observed that the left and right contact angles remains constant within the experimental error, up to T = 89°C. At this temperature a quite violent explosion is observed which makes the drop no longer distinguishable. Figure 41 shows the lateral profile of the drop at different temperatures. We note the presence of two drops, on the left there is a small size drop created during the deposition of the liquid crystal on the substrate while on the right there is the larger size drop used for the experiment (Fig.41-A). As already mentioned, the contact angle during the entire cooling phase doesn't undergo large variations and can also be seen from the shape of the drop (Fig.41-B and

Fig.41-C). At T=89°C a quiet violent explosion takes place and the typical dome shape of the drop is no longer present (Fig.41-D). The small drop exploded as well, at the same temperature.

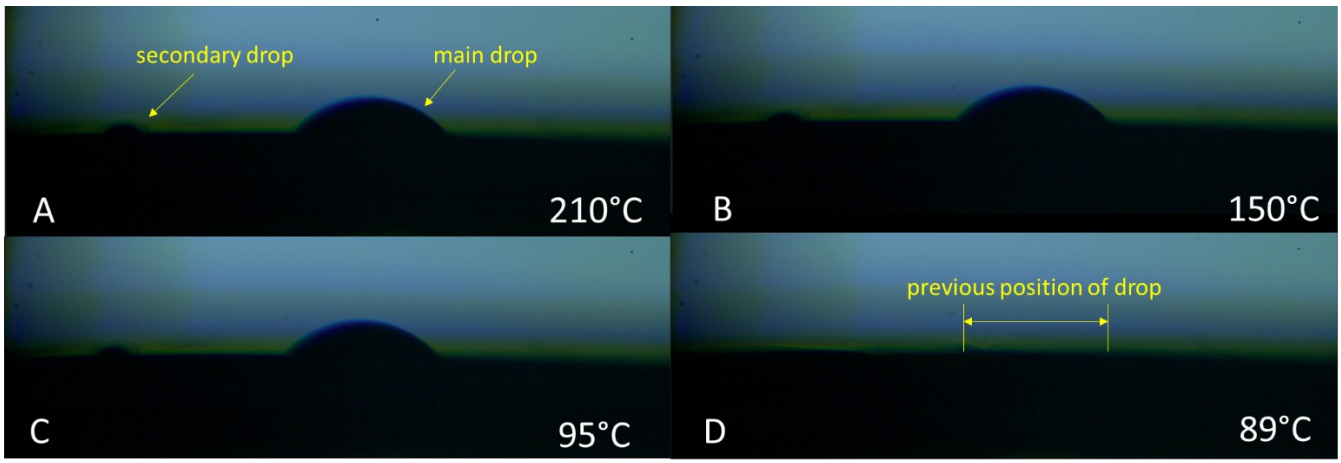

Figure 41. Droplet side profile of RM734 on Fe:$LiNbO_3$ (R=1.05) substrate at different temperatures

CHAPTER 5

5. Discussion

In this chapter we will discuss the results reported in the previous chapter, with specific attention to the peculiar phenomena that we observed and to the limits of our experimental approach.

The first observed property of RM734 sessile droplets is the difference between the right and left contact angles. This difference is visible from the beginning of the experiments and is probably due to the way we use to deposit the drop on the substrate. In fact, this could cause an asymmetry in the shape of the drop. The difference in the trend between the two angles during the experiment, on the other hand, may be due to the ejection of jets. Indeed, after the expulsion of the material, the drop tends to minimize the surface energy finding a more spherical shape by making the two angles uniform and this can lead to an asymmetry between them. Figure 42 reports the average value of the contact angle, for all the seven substrates we analyzed.

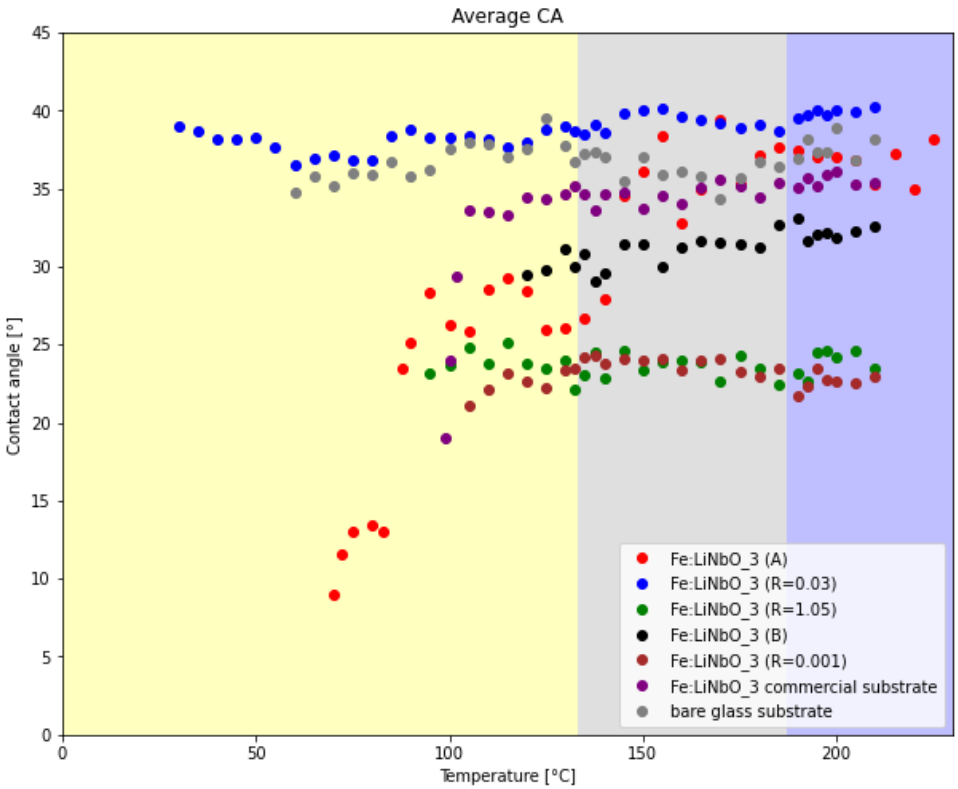

Figure 42. Average contact angle graph of RM734 on all substrates

As described in chapter 4, two of the seven substrates (the bare glass and the Fe:$LiNBO_3$ (R=0.03)) didn't give rise to the RM734 droplets instability. This was expected for the bare glass, which doesn't produce any electric field that can interact with the NF droplet, but quite surprising for the Fe:$LiNBO_3$ (R=0.03) substrate. As for the other LN substrates, although with all of them the NF

droplets undergo one or more instability event, this is not characterized by a common behavior of the wettability. Specifically, with the substrates: Fe:$LiNBO_3$ diffused doped (B) and Fe:$LiNBO_3$ (R=1.05), the average contact angle stays approximately constant up to the onset of the electromechanical instability, which led in these cases to violent explosion resulting in a total loss of the droplet's dome shape. For the Fe:$LiNBO_3$ commercial undoped substrate and Fe:$LiNBO_3$ (R=0.001) substrate the average contact angle remains constant before instability which is preceded by the manifestation of ejection of fluid jets coming out of the drop of RM734. On the Fe:$LiNBO_3$ diffused doped substrate (A) the contact angle undergoes large variations before the manifestation of jet ejection.

RM734 droplets on Fe:$LiNBO_3$ diffused doped substrate (A) and Fe:$LiNBO_3$ (R=0.03) substrate have shown a peculiar behavior compared to the other experiments. These behaviors will be discussed in the following sections.

5.1 Fe:$LiNbO_3$ DIFFUSED DOPED (A) SUBSTRATE CASE

Fe:$LiNbO_3$ diffused doped (A) was the experiment where the contact angle values changed the most. During the cooling ramp there were several significant events up to the final explosion in which the typical drop shape was no longer distinguishable. Figure 43 shows the main steps of the instability of the RM734 sample until to the arrival of the final explosion.

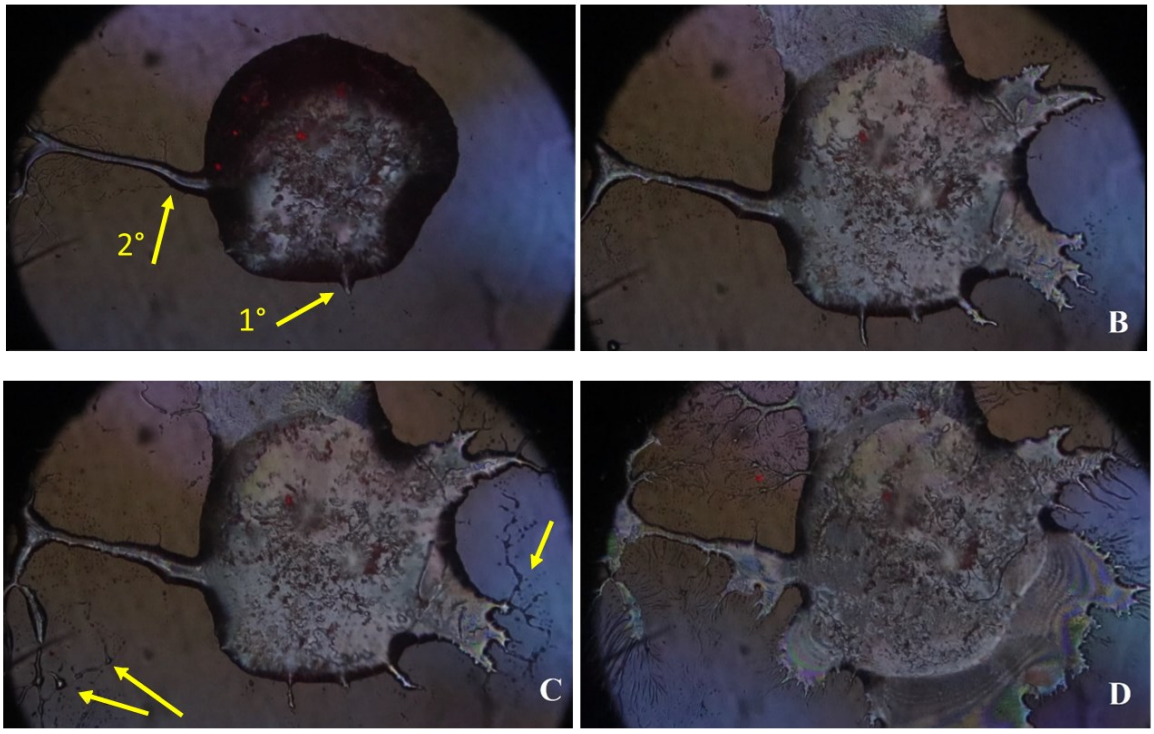

Figure 43. Instability phases RM734 on the substrate Fe:$LiNbO_3$ diffused doped (A)

From the starting temperature, a change in surface texture was observed at temperature of 170°C, which indicates that the liquid crystal is in the nematic phase. The first jet of fluid took place at 95°C followed immediately after by another jet of larger dimensions (fig. 43-A), after this phase, by lowering the temperature, a "non-violent" explosion is observed, figure 43-B. This involves a deformation of the droplet shape. The tendency of the expelled jets' tips to bifurcate, creating branched structures with multiple layers of ramification, suggests that they are unstable themselves. The formation of many small secondary droplets can be seen in the figure 43-C. Upon lowering T further, new additional instabilities are observed involving the mother droplet and the secondary droplets. In fact, at the temperature of 88°C, the explosions of the secondary drops and the violent explosion of the mother drop can be observed at the same time (figure 43-D). What happened in this experiment differs from the others due to the formation of numerous jets, secondary drops and the multiple explosions that took place at different temperatures.

5.2 Fe:$LiNbO_3$ (R=0.03) SUBSTRATE CASE

The experiment on this substrate gave a very different final result compared to the other experiments carried out on other substrates. Indeed, the drop of RM734 did not become unstable and did not explode. The experiment was repeated and the final result was always the same. In the first experiment a cooling ramp equal to that of the other experiments was used. Then, we decided to give a higher ΔT to the RM734 sample, therefore from the temperature of 45°C we returned to 120°C and the plate resistances were switched off to have a sudden drop in temperature. Again, we returned to room temperature and the droplet doesn't show any evidence of instability such as jets or deformation. The last attempt to induce instability was carried out by bringing the temperature of the plate with the drop back to a temperature of 150°C and dropping again abruptly to a temperature of 20°C but this attempt also didn't induce the explosion.
A tentative interpretation of this effect can be found in the amount of iron present in the substrate. The Fe:$LiNBO_3$ (R=0.03) is the one with the highest level of iron doping and we can reasonably expect this to lead to the highest value of the thermal conductivity. A high thermal conductivity can produce a rapid thermalization of the crystal, which, as a consequence, generates a low and rapidly vanishing pyroelectric field.

Another interesting observation is related to the average values of the contact angles in the isotropic phase. They are quite low in all our experiments, assuming the lowest values in two cases: the one with the highest value of R and the one with the highest content of iron. This seems to indicate that a large amount of Fe2+ ions lead to a high wettability of the crystal surface.
As for the role of the variation of the drop surface tension due to the Coulomb repulsion between the polarization charges deposited on the droplet surfaces as it enters the NF phase, our results show that this behavior is not common to all the experiments. In some case, the drop shape instability takes place without a previous decrease of the surface tension showing that this effect is not as crucial as we predicted, probably because the droplet charging stays quite low until jet ejection occurs. In this scenario, the relevant effect is just charge accumulation in correspondence of the topological defects.

5.3 PECULIAR PHENOMENON OBSERVED

A particular phenomenon was observed at the end of the experiment on substrate Fe:$LiNbO_3$ (R=0.001). Moving the substrate from the position in which the experiment was execute, we could also observe tree-like jets developing vertically from the droplet (Fig.44). At the moment we don't know the causes that led to the creation of this kind of jet.

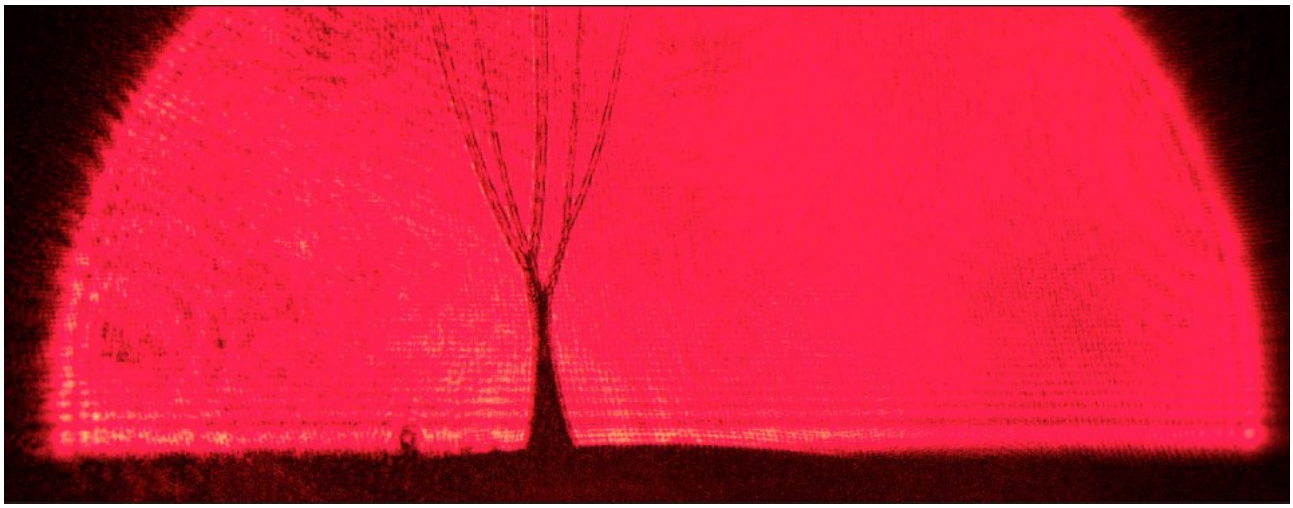

Figure 44. Particular phenomenon observed

5.4 LIMITS OF THE EXPERIMENTAL PROCEDURE

Our experimental procedure revealed limitations, which will be discussed in this section.

The first limitation is that the experiments carried out in the laboratory were performed in an open environment at room temperature and the drop was not isolated. This results in a difference between the measured temperatures on the plate by the probe and the temperature of the droplet on the substrate, that may have led to phase transition temperatures different from those known in the literature. The confirmation is given to us by observing how the green laser light spreads in the drop of RM734. Light scatters differently in the isotropic phase, nematic phase and ferroelectric nematic phase. Figure 45 shows how the laser light spreads differently in the different transition phases.

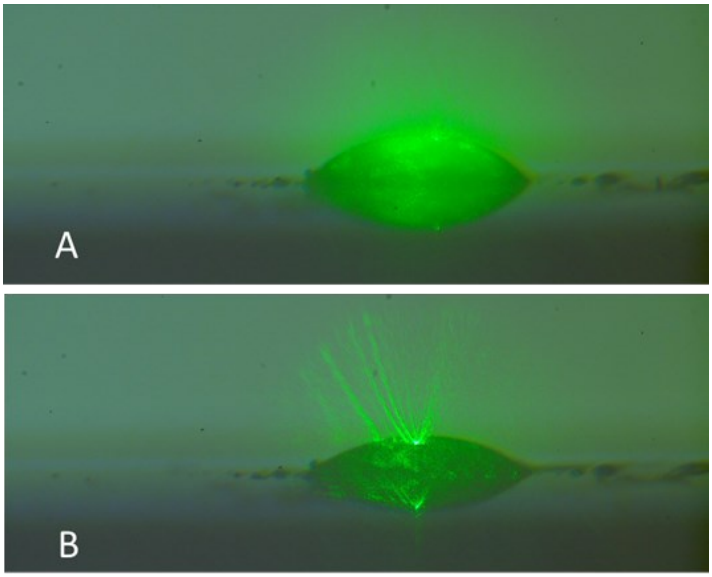

Figure 45. Diffused light through the drop in different transition phases

In figure 45-A the drop of liquid crystal is exposed to a temperature of 210°C which corresponds to the nematic phase while in figure 45-B the liquid crystal is in the ferroelectric nematic phase at temperature of 155°C. In the literature these two phases are indicated respectively at the temperature of 187°C and 133°C, this indicates a difference between the theoretical temperatures and the measured temperatures.

The second limit concerns the sequence of software used. ImageJ with the registered function fixes the same baseline for all the images but sometimes this function can't be applied to all the photos. This implies that when we import the images processed by ImageJ to Ossila for the contact angle calculation, for the sequence of images in which the registered function could not be applied, we have to manually position the lines that interpolate the drop for the contact angle calculation. As a result you may run into accuracy issues. This was verified by comparing the same experiments once carried out with the registered function, consequently Ossila automatically calculated the contact angles, while the counter-test with images without the registered function and on Ossila the lines that interpolate the drop were manually positioned for each frame to obtain the contact angle. On average, a difference between the two cases of 3° was calculated.

CHAPTER 6

Conclusion and future goals

The analysis carried out in the previous sections made it possible to determine the variation of the contact angle of the RM734 ferroelectric liquid crystal on various types of ferroelectric substrates. Through a heated plate on which the substrate with the RM734 droplet was placed, it was possible to bring the liquid crystal to different temperatures so that it goes from the isotropic phase, to the nematic and finally to the ferroelectric nematic phase. This study highlighted phenomena such as those recently reported [3] related to the instability that led to the explosion of ferroelectric liquid crystal drops.

The idea behind the study of wettability on different types of lithium niobate crystals, was born to verify an observation made during a study of the instability reported in the PNAS article [7]. In this article it is reported that the instability is preceded by a strong decrease of the contact angle when the liquid crystal enters the ferroelectric phase and this decrease is due to a variation of the surface tensions generated by the accumulation of charge on the surface of the drop. To test this hypothesis in detail, we studied the wettability of RM734 on different types of lithium niobate crystals and, for comparison, on bare glass.

For each experiment, both left and right contact angles of the drop were measured and their average value was calculated. The average contact angles have been reported on graphs as a function of temperature.

Results demonstrate that the ejection of jets is not always preceded by a strong decrease in the contact angle, which indicates that the variation of the surface tension due to droplet charging can be quite small even in the ferroelectric nematic phase.

From this we can deduced that the variation of surface tension at the droplet-air interface has a non-dominant role and therefore the instability is mainly driven by the accumulation of charge in the topological defects.

This study is motivated by the need of characterizing the coupling between the polarization of the solid (lithium niobate) and the polarization of the liquid crystal (RM734). Such a coupling between fluid and solid ferroelectric materials has never been observed before. As such its study is highly desirable from both a fundamental and an applicative point of view.

The discovery of the ferroelectric nematic phase has attracted the attention of many researchers coming from different fields. and One of the foreseen possible applications is related to the design of innovative electric charge accumulators based on the negative capacitance of capacitors containing ferroelectric liquid crystals. The great advantage of using ferroelectrics in the liquid phase is linked to the large spontaneous polarization **P** that these materials exhibit and which respond to electric fields up to six orders of magnitude lower than those used with more traditional solid ferroelectrics. In fact, like all liquid crystals, they have a high degree of orientational freedom, which can be exploited for the accumulation of surface charge.

This is also related to the very hot theme of "green energy". Indeed, the well-known capability of liquid crystals to be easily polarized by light might in principle be exploited for the direct conversion of light energy into electrostatic energy in Negative Liquid Ferroelectric Capacitors. By placing the ferroelectric liquid in thin layers alternating with dielectrics and conductive materials, it might be possible to demonstrate that negative capacitors could accumulate charge by exploiting the polarization induced by light, converting it directly into electrical energy. This very ambitious goal could revolutionize the world of green energy production and conservation; it would result in an innovative and completely clean way of producing directly-available electric charge inside accumulators for possible applications: thus, a set of photovoltaic panels and accumulators in a single tool, directly available to be used, even overcoming the natural limitations of photovoltaic systems that strongly depend on the level of available lighting.
Due to the peculiar properties of ferroelectric liquids, many other applications can be envisaged as for example ferroelectric memories based on hybrid solid/liquid devices or highly sensitive sensors. In this context of great ferment in the investigation of the behavior of ferroelectric liquid crystals, my research work contributes to adding new knowledge on the behavior of these materials.

Bibliography

[1] De Gennes P., Prost J., *The physics of Liquid Crystals,* Oxford science publications, Clarendon Press, 1993.

[2] Mandle R., *A new order of liquids: polar order in nematic liquid crystals*, Soft Matter, 8, 5014-5020, 2022.

[3] Barboza R., Marni S., Ciciulla F., Lucchetti L., *Explosive electrostatic instability of ferroelectric liquid droplets on ferroelectric solid surface*, PNAS, Vol.119, No.32, August 9, 2022.

[4] Priestely E., Wojtowicz P. Sheng P., *Introduction to liquid crystals*, RCA laboratories, Princeton, USA, 1975.

[5] Osipova M., Gorkunov M., *Microscopic origin of ferroelectricity in chiral smectic C* liquid crystals and ordering of 'ferroelectric fishes' proposed by de Gennes,* Liquid Crystals, Vol. 36, Nos. 10–11, October–November 2009.

[6] Kuczynski W., Stegemeyer H., *Ferroelectric properties of smectic c liquid crystals with induced helical structure,* Chemical Physics Letters, Vol.70, n°1, 1980.

[7] García-Cabañes A., Blázquez-Castro A., Arizmendi L., Agulló-López F. e Carrascosa M., *Recent Achievements on Photovoltaic Optoelectronic Tweezers Based on Lithium Niobate*, in *Crystals*, 2018.

[8] Damjanovic D., (1998). *Ferroelectric, dielectric and piezoelectric properties of ferroelectric thin films and ceramic*, Report on progress in Physics, Vol 61 (9): 1267–1324, 1998.

[9] Xi Chen, Eva Korblova, Noel A. Clark, *First-principles experimental demonstration of ferroelectricity in a thermotropic nematic liquid crystal: Polar domains and striking electro-optics*, Vol.117, PNAS, 2020.